Applied Numerical Mathematics 62 (2012) 1393–1410

Contents lists available at SciVerse ScienceDirect

Applied Numerical Mathematics

www.elsevier.com/locate/apnum

Presentation and comparison of selected algorithms for dynamic contact based on the Newmark scheme ☆

Rolf Krause [a,*], Mirjam Walloth [b]

[a] Institute of Computational Science, Università della Svizzera Italiana, via Giuseppe Buffi 13, CH-6900 Lugano, Switzerland
[b] Institute for Numerical Simulation, University of Bonn, Wegelerstraße 6, D-53115 Bonn, Germany

ARTICLE INFO

Article history:
Available online 7 June 2012

Keywords:
Dynamic contact problems
Elasticity
Rothe's method
Stability

ABSTRACT

The straightforward application of classical time discretization schemes to dynamic contact problems often leads to instabilities at the contact boundary. These show up as artificial oscillations in the contact stresses and displacements at the contact boundary, or an uncontrollable behavior of the total energy. During the last years, several new discretization schemes for contact problems have been developed, which are designed to avoid an instable behavior of the discrete evolution. As a matter of fact, many of these methods are based on one of the most popular time discretization schemes in structural dynamics, the Newmark scheme. Here, we present these algorithms in a consistent notation and discuss the advantages and disadvantages of the respective approaches. Our unifying presentation allows furthermore for a deeper insight into the causes of the instabilities, providing physical as well as formal explanations for an instable behavior of the discrete evolutions. Numerical examples in 3D illustrate the effects of the different methods.

0. Introduction

One of the most common time discretizations in structural dynamics is the classical Newmark scheme. It is of second order accuracy and conserves the energy in the unconstrained case. Therefore, it seems to be natural to use the classical Newmark scheme for dynamic problems under constraints. Unfortunately, in the case of contact constraints, the classical Newmark scheme evokes oscillations in the contact stresses, the displacements and the velocities at the contact boundary and even energy blow-ups may occur which spoil the accuracy of the solution. Reasons can be found in the interaction of the time and space discretization, in the violation of the persistency condition and in the discrete change of the velocity at the moment of impact. We give a deeper insight into the causes of these instabilities. In order to avoid this unstable behavior of the discrete evolution, many time discretizations, especially modifications of the Newmark scheme have been developed. In a unifying framework we present several approaches and discuss the ideas and the pros and cons of the different algorithms.

Our survey will focus on the following recent approaches: Algorithms improving the Newmark method with special regard to the conservation of energy are presented by Laursen and Chawla in 'Design of energy conserving algorithms for frictionless dynamic contact problems' [23] and by Laursen and Love in 'Improved implicit integrators for transient impact problems — geometric admissibility within the conserving framework' [24]. Methods primarily reducing the oscillations in the contact forces are described by Deuflhard, Krause and Ertel in 'A contact-stabilized Newmark method for dynamical

☆ This work was supported by the SFB 611 "Singular Phenomena and Scaling in Mathematical Models" and by the Hausdorff-Center for Mathematics, Bonn.

* Corresponding author.
E-mail addresses: rolf.krause@usi.ch (R. Krause), walloth@ins.uni-bonn.de (M. Walloth).

0168-9274/$36.00 © 2012 IMACS. Published by Elsevier B.V. All rights reserved.
http://dx.doi.org/10.1016/j.apnum.2012.06.014

contact problems' [4] and by Khenous, Laborde and Renard in 'Mass redistribution method for finite element contact problems in elastodynamics' [14]. In 'A stable energy conserving approach for frictional contact problems based on quadrature formulas' [9] by Hager, Hüeber and Wohlmuth, the key ideas of [23] and [14] are both taken into account and improved concerning the numerical costs.

In the last section numerical results for one- and two-body contact problems demonstrate the merits and drawbacks of the different algorithms.

1. Dynamic two-body contact — Formulation and conservation properties

In this section, we give the strong and the variational formulation of a dynamic two-body contact problem in linear elasticity. After introducing the non-penetration constraints modeling the contact we first state the strong formulation. Then, the weak formulation of this dynamic contact problem is derived which leads to a hyperbolic variational inequality. Finally, we discuss conservation properties of the system (i.e., conservation of energy or momentum), which play an important role for the construction of suitable time discretization schemes.

1.1. Strong formulation of dynamic two-body contact

We consider two elastic bodies, which, subjected to initial velocities or to body and surface forces, will collide and undergo some displacements $\boldsymbol{u}$. The bodies in their reference configurations are identified with the polyhedral domains $\Omega^K \subset \mathbb{R}^d$, $d = 2, 3$, and $K \in \{S, M\}$ where S and M stand for slave and master body, respectively. We remark that this notation is borrowed from the context of Mortar methods, see, e.g. [29]. According to this decomposition $\Omega = \Omega^S \cup \Omega^M$, the sought displacements are $\boldsymbol{u} = (\boldsymbol{u}^S, \boldsymbol{u}^M)$. Each of the boundary segments $\Gamma^K := \partial\Omega^K$ has a possible contact boundary $\Gamma_C^K \subset \Gamma^K$. The actual contact boundary is not known in advance but is assumed to be contained in a compact strict subset of Γ_C^K. We set $\Gamma_C := \Gamma_C^S \cup \Gamma_C^M$.

Tensor and vector quantities are written in bold characters, e.g., the stress tensor $\boldsymbol{\sigma}$ and the displacement $\boldsymbol{u}$ with components σ_{ij} and u_i. The summation convention is enforced on all repeated indices.

The two bodies consist of linear elastic materials [3]. This means that the strain is described by the linearized strain tensor $\boldsymbol{\epsilon}(\boldsymbol{u}^K) := \frac{1}{2}(\nabla \boldsymbol{u}^K + (\nabla \boldsymbol{u}^K)^T)$ and the stress tensor $\boldsymbol{\sigma}$ obeys Hooke's law

$$\sigma_{ij}\left(\boldsymbol{u}^K\right) := E_{ijml}^K \epsilon_{ml}^K \tag{1}$$

where Hooke's tensor $\boldsymbol{E}^K = (E_{ijml}^K)$ is sufficiently smooth, $E_{ijml}^K \in L^\infty(\Omega)$, and is symmetric and uniformly positive definite. In this case, the elastic potential energy is induced by means of the bilinear-form

$$a(\boldsymbol{u}, \boldsymbol{u}) := \sum_{K\in\{S,M\}} \int_{\Omega^K} \boldsymbol{\sigma}\left(\boldsymbol{u}^K\right) : \boldsymbol{\epsilon}\left(\boldsymbol{u}^K\right) dx. \tag{2}$$

At the contact boundary the two bodies must not penetrate each other. Therefore, the displacements have to fulfill a non-penetration condition. For small deformations as considered here, usually a linearized non-penetration condition, see [15], is employed. In order to derive this linearized non-penetration condition, we assume a bijective and sufficiently smooth mapping $\boldsymbol{\phi} : \Gamma_C^S \to \Gamma_C^M$ between the two possible contact surfaces to be given. Then, the function $g(\boldsymbol{x}) := \|\boldsymbol{x} - \boldsymbol{\phi}(\boldsymbol{x})\|$, $\boldsymbol{x} \in \Gamma_C^S$, describes the initial gap and the unit outward normal is

$$\boldsymbol{\nu}_\phi(\boldsymbol{x}) := \begin{cases} \frac{\boldsymbol{\phi}(\boldsymbol{x})-\boldsymbol{x}}{\|\boldsymbol{\phi}(\boldsymbol{x})-\boldsymbol{x}\|}, & \text{if } \boldsymbol{x} \neq \boldsymbol{\phi}(\boldsymbol{x}) \\ \boldsymbol{\nu}^S(\boldsymbol{x}) = -\boldsymbol{\nu}^M(\boldsymbol{x}), & \text{if } \boldsymbol{x} = \boldsymbol{\phi}(\boldsymbol{x}). \end{cases}$$

Here and in the following, $\|\cdot\|$ denotes the Euclidean norm. We now define the linearized non-penetration condition

$$[\boldsymbol{u}\cdot\boldsymbol{\nu}_\phi]_\phi(\boldsymbol{x}, t) := \boldsymbol{u}^S(\boldsymbol{x}, t)\cdot\boldsymbol{\nu}_\phi(\boldsymbol{x}) - \boldsymbol{u}^M\left(\boldsymbol{\phi}(\boldsymbol{x}), t\right)\cdot\boldsymbol{\nu}_\phi(\boldsymbol{x}) \leqslant g(\boldsymbol{x}) \quad \forall \boldsymbol{x} \in \Gamma_C^S. \tag{3}$$

Let us note that, by means of the bijection $\boldsymbol{\phi}$, points on Γ_C^S and Γ_C^M, which may come into contact, are identified a priori. Under the assumptions, that the contact boundaries on slave and master side are close and that $\boldsymbol{\nu}^S \approx -\boldsymbol{\nu}^M \approx \boldsymbol{\nu}_\phi$, which are fulfilled for small deformations, the approximation error caused by the linearized non-penetration condition is analyzed in [6]. For the case of large deformations, the non-penetration condition depends highly non-linearly on the displacements $\boldsymbol{u}$. Concepts for the numerical solution of large deformation contact problems can be found, e.g., in [22]. For a recent approach, we refer to [20] where a signed distance function is applied instead of the mapping $\boldsymbol{\phi}$.

We set $\boldsymbol{\nu} := \boldsymbol{\nu}_\phi \approx \boldsymbol{\nu}^S \approx -\boldsymbol{\nu}^M$ and $[\boldsymbol{u}\cdot\boldsymbol{\nu}] := [\boldsymbol{u}\cdot\boldsymbol{\nu}_\phi]_\phi$ which is the jump of $\boldsymbol{u}$ in normal direction at the interface. Further we define the contact stresses by

$$\hat{\boldsymbol{\sigma}}\left(\boldsymbol{u}^K\right) := \boldsymbol{\sigma}\left(\boldsymbol{u}^K\right)\cdot\boldsymbol{\nu}^K$$

and their normal component by

$$\sigma_\nu := \nu_i^S \cdot \sigma_{ij}\big(\boldsymbol{u}^S\big) \cdot \nu_j^S.$$

Now we are in a position to give the strong formulation of the dynamic two-body contact problem. This formulation consists of the equation of motion (4), the contact conditions (5)–(8) and the initial data (9).

$$\rho \ddot{u}_i - \sigma_{ij}(\boldsymbol{u})_{,j} = \rho f_i \quad \text{in } \Omega \times [0,T] \tag{4}$$

$$\hat{\boldsymbol{\sigma}}\big(\boldsymbol{u}^M \circ \boldsymbol{\phi}\big) = -\hat{\boldsymbol{\sigma}}\big(\boldsymbol{u}^S\big) \quad \text{on } \Gamma_C^S \times [0,T] \tag{5}$$

$$\sigma_\nu \leqslant 0 \quad \text{on } \Gamma_C^S \times [0,T] \tag{6}$$

$$[\boldsymbol{u} \cdot \boldsymbol{\nu}] \leqslant g \quad \text{on } \Gamma_C^S \times [0,T] \tag{7}$$

$$\big([\boldsymbol{u} \cdot \boldsymbol{\nu}] - g\big)\sigma_\nu = 0 \quad \text{on } \Gamma_C^S \times [0,T] \tag{8}$$

$$\boldsymbol{u}(\boldsymbol{x},0) = \boldsymbol{u}_0(\boldsymbol{x}), \qquad \dot{\boldsymbol{u}}(\boldsymbol{x},0) = \dot{\boldsymbol{u}}_0(\boldsymbol{x}) \quad \text{in } \Omega \tag{9}$$

Here, $\rho > 0$ is the density and $\rho \boldsymbol{f}$ the volume force density. Besides volume forces, surface tractions $\sigma_{ij}(\boldsymbol{u}) \cdot \nu_j = \pi_i$ on $\Gamma_N \times [0,T]$ and Dirichlet values on $\Gamma_D \times [0,T]$ could be applied. Γ_N^K and Γ_D^K are the Neumann and Dirichlet boundaries on the slave ($K = S$) and master sides ($K = M$). The Dirichlet, Neumann and contact boundaries have to be disjoint parts of the whole boundary Γ^K. For the ease of presentation we assume in the following, that we have no Dirichlet boundary.

We remark that in contrast to the static case, for the above given dynamic problem many questions regarding the solution and its possible properties are still open, see e.g., [7]. Throughout this paper, we therefore simply assume that a solution of the above stated problem exists.

In this article, we focus on the frictionless case, but as we like to comment shortly on the extensibility of the algorithms to frictional contact, we introduce the Coulomb friction law. Therefore, it is useful to have the definitions $u_\nu := \boldsymbol{u} \cdot \boldsymbol{\nu}$ and $\boldsymbol{u}_T := \boldsymbol{u} - u_\nu \cdot \boldsymbol{\nu}$ for the normal and tangential component of a vector $\boldsymbol{u}$. We define the jump in tangential direction

$$[\boldsymbol{u}_T] := \boldsymbol{u}^S(\boldsymbol{x},t) - u_\nu^S(\boldsymbol{x},t) \cdot \boldsymbol{\nu} - \big(\boldsymbol{u}^M\big(\boldsymbol{\phi}(\boldsymbol{x}),t\big) - u_\nu^M\big(\boldsymbol{\phi}(\boldsymbol{x}),t\big) \cdot \boldsymbol{\nu}\big)$$

and the tangential contact stresses $\boldsymbol{\sigma}_T := \hat{\boldsymbol{\sigma}}(\boldsymbol{u}^S) - \sigma_\nu \cdot \boldsymbol{\nu}$. The Coulomb friction law is given by

$$\begin{aligned} &[\dot{\boldsymbol{u}}_T] = 0 \quad \Rightarrow \quad \|\boldsymbol{\sigma}_T\| \leqslant \mathcal{F}|\sigma_\nu| \quad \text{on } \Gamma_C^S \times [0,T] \\ &[\dot{\boldsymbol{u}}_T] \neq 0 \quad \Rightarrow \quad \boldsymbol{\sigma}_T = -\mathcal{F}|\sigma_\nu| \frac{[\dot{\boldsymbol{u}}_T]}{\|[\dot{\boldsymbol{u}}_T]\|} \quad \text{on } \Gamma_C^S \times [0,T] \end{aligned} \tag{10}$$

where $\mathcal{F} \geqslant 0$ is the coefficient of friction.

1.2. Variational formulation of dynamic two-body contact

Within the weak formulation of the dynamic contact problem (4)–(9), as solution space for the spatial variables we take the product space $\boldsymbol{H}^1 = \boldsymbol{H}^1(\Omega^S) \times \boldsymbol{H}^1(\Omega^M)$. Here, we have set $\boldsymbol{H}^1(\Omega^K) := (H^1(\Omega^K))^d$. We furthermore need the closed and convex set

$$\mathcal{K} := \big\{ \boldsymbol{v} \in \boldsymbol{H}^1 \,\big|\, [\boldsymbol{v} \cdot \boldsymbol{\nu}] \leqslant g \big\} \subset \boldsymbol{H}^1.$$

Let us note that the definition of $\mathcal{K}$ makes use of the trace operators $\mathrm{tr}_K \colon \boldsymbol{H}^1(\Omega^K) \to \boldsymbol{H}^{1/2}(\partial\Omega^K)$. As a consequence, the set $\mathcal{K}$ of admissible displacements is well defined in $\boldsymbol{H}^1$ but not in, e.g., $\boldsymbol{L}^2 = \boldsymbol{L}^2(\Omega^S) \times \boldsymbol{L}^2(\Omega^M)$. This simple observation will be of interest later on, when we present in Section 3.5 the contact-stabilized Newmark scheme, introduced in [4].

For the volume force density we assume $\rho \boldsymbol{f}(\cdot,t) \in \boldsymbol{L}^2$ for all $t \in [0,T]$, and the $\boldsymbol{L}^2$-scalar product $(\cdot,\cdot) = (\rho\cdot,\cdot)_{L^2}$ is understood to be weighted by the density $\rho_{\max} \geqslant \rho(\boldsymbol{x}) \geqslant \rho_{\min} > 0$.

The weak formulation of the frictionless dynamic contact problem is a hyperbolic variational inequality which is derived from the strong formulation via integrating by parts and exploiting the non-penetration condition: For every $t \in (0,T]$ find $\boldsymbol{u}(\cdot,t) \in \boldsymbol{H}^1$ with $\ddot{\boldsymbol{u}}(\cdot,t) \in \boldsymbol{L}^2$, so that

$$(\ddot{\boldsymbol{u}}, \boldsymbol{v} - \boldsymbol{u}) + a(\boldsymbol{u}, \boldsymbol{v} - \boldsymbol{u}) + \mathcal{I}_{\mathcal{K}}(\boldsymbol{v}) - \mathcal{I}_{\mathcal{K}}(\boldsymbol{u}) \geqslant (\boldsymbol{f}, \boldsymbol{v} - \boldsymbol{u}) \quad \forall \boldsymbol{v} \in \boldsymbol{H}^1 \tag{11}$$

where

$$\mathcal{I}_{\mathcal{K}}(\boldsymbol{v}) = \begin{cases} 0, & \text{if } \boldsymbol{v} \in \mathcal{K} \\ \infty, & \text{otherwise} \end{cases}$$

is the characteristic functional. With the definition $(\boldsymbol{F}(\boldsymbol{u}),\cdot) := a(\boldsymbol{u},\cdot) - (\boldsymbol{f},\cdot)$ and the subdifferential $\partial\mathcal{I}_{\mathcal{K}}(\boldsymbol{u})(\cdot)$ we can rewrite (11) as

$$0 \in (\ddot{\boldsymbol{u}},\cdot) + \big(\boldsymbol{F}(\boldsymbol{u}),\cdot\big) + \partial\mathcal{I}_{\mathcal{K}}(\boldsymbol{u})(\cdot) \tag{12}$$

cf. [8] for variational inclusions. The interpretation of the subdifferential in the case of contact is of crucial importance for understanding the difficulties connected to the discretization in time and space. Let us assume that $\boldsymbol{u}$ is a solution of the variational inequality (11). Then, Green's formula implies that for each fixed t we have

$$(\ddot{\boldsymbol{u}}, \boldsymbol{v}) + \big(\boldsymbol{F}(\boldsymbol{u}), \boldsymbol{v}\big) = \big(\hat{\boldsymbol{\sigma}}(\boldsymbol{u}), \boldsymbol{v}\big)_{L^2(\Gamma_C)} \tag{13}$$

which shows that $\hat{\boldsymbol{\sigma}}(\boldsymbol{u})$ plays the role of a Lagrange multiplier for (11). Lagrange multipliers will be denoted by $\boldsymbol{\lambda}$ throughout this article. We emphasize that $\hat{\boldsymbol{\sigma}}(\boldsymbol{u})$ is a priori unknown and has to be determined as a part of the solution process. We define the so-called contact forces by means of $(\boldsymbol{F}_{\mathrm{con}}(\boldsymbol{u}), \boldsymbol{v})_{L^2(\Omega)} := (\hat{\boldsymbol{\sigma}}(\boldsymbol{u}), \cdot)_{L^2(\Gamma_C)}$ and we reformulate Eq. (13) as

$$\big(\boldsymbol{F}_{\mathrm{con}}(\boldsymbol{u}), \boldsymbol{v}\big) = \big(\ddot{\boldsymbol{u}} + \boldsymbol{F}(\boldsymbol{u}), \boldsymbol{v}\big) \tag{14}$$

which reminds us of Newton's equation of motion. Therefore, from now on we call $\boldsymbol{F}_{\mathrm{con}}$ the contact forces and we refer to $\boldsymbol{F}$ as forces. Comparing (12) and (14) we figure out that $-\boldsymbol{F}_{\mathrm{con}}(\boldsymbol{u}) \in \partial \mathcal{I}_{\mathcal{K}}(\boldsymbol{u})$.

1.3. Conservation properties

In this subsection we show how the contact constraints influence the conservation properties of the system. In general energy is conserved as long as the volume forces are conservative forces. Then the potential energy is given by $\mathcal{E}_{\mathrm{pot}}(\boldsymbol{u}) := \frac{1}{2}a(\boldsymbol{u}, \boldsymbol{u}) + (\boldsymbol{f}, \boldsymbol{u}) \in \mathbb{R}$ and $\mathcal{E}_{\mathrm{kin}}(\boldsymbol{u}) := \frac{1}{2}(\dot{\boldsymbol{u}}, \dot{\boldsymbol{u}}) \in \mathbb{R}$ is the kinetic energy. We will see that the so-called persistency condition

$$\sigma_\nu \frac{d}{dt}[\boldsymbol{u} \cdot \boldsymbol{v}] = 0 \quad \text{on } \Gamma_C^S \tag{15}$$

which says that in the case of contact the relative velocities in normal direction at the contact boundary have to be zero is essential for the energy conservation for contact problems. It is easy to imagine that these relative velocities are zero if the contact boundaries stick together. But as we will see later on it is difficult to realize this condition in the fully discrete setting. In order to derive the persistency condition, we use $\dot{\boldsymbol{u}}$, assuming that it is sufficiently smooth, as trial function in Eq. (13).

$$\begin{aligned} 0 &= \int_\Omega \boldsymbol{\sigma}(\boldsymbol{u}) : \boldsymbol{\epsilon}(\dot{\boldsymbol{u}})\, dx + \int_\Omega \rho \ddot{\boldsymbol{u}} \cdot \dot{\boldsymbol{u}}\, dx - \int_\Omega \rho \boldsymbol{f} \cdot \dot{\boldsymbol{u}}\, dx - \int_{\Gamma_C^S} \hat{\boldsymbol{\sigma}}\big(\boldsymbol{u}^S\big)\big(\dot{\boldsymbol{u}}^S - \dot{\boldsymbol{u}}^M \circ \boldsymbol{\phi}\big)\, dx \\ &= \frac{d\mathcal{E}(\boldsymbol{u})}{dt} - \int_{\Gamma_C^S} \hat{\boldsymbol{\sigma}}\big(\boldsymbol{u}^S\big)\big(\dot{\boldsymbol{u}}^S - \dot{\boldsymbol{u}}^M \circ \boldsymbol{\phi}\big)\, dx \end{aligned}$$

It is evident that the energy is conserved if the persistency condition (15) is fulfilled. In the case of friction, when $\boldsymbol{\sigma}_T \neq 0$ holds, we can deduce that friction evokes dissipation, due to the fact that either $[\dot{\boldsymbol{u}}_T] = \boldsymbol{0}$ or $\boldsymbol{\sigma}_T = -\mathcal{F}|\sigma_\nu| \frac{[\dot{\boldsymbol{u}}_T]}{\|[\dot{\boldsymbol{u}}_T]\|}$.

Other conserved quantities are the linear momentum and the angular momentum. For the proof of the conservation of the linear momentum $\boldsymbol{\mathcal{L}}(\boldsymbol{u}) = (\dot{\boldsymbol{u}}, 1) \in \mathbb{R}^d$ we solely have to exclude that the system is exposed to external forces. We take a constant trial function $\boldsymbol{w} \in \boldsymbol{H}^1$ in Eq. (14) and use the identity $\int_\Omega \rho \boldsymbol{f} = 0$ for internal forces.

$$\begin{aligned} 0 &= \int_\Omega \boldsymbol{\sigma}(\boldsymbol{u}) : \boldsymbol{\epsilon}(\boldsymbol{w})\, dx + \int_\Omega \rho \ddot{\boldsymbol{u}} \cdot \boldsymbol{w}\, dx - \int_\Omega \rho \boldsymbol{f} \cdot \boldsymbol{w}\, dx - \int_{\Gamma_C^S} \hat{\boldsymbol{\sigma}}\big(\boldsymbol{u}^S\big)(\boldsymbol{w} - \boldsymbol{w})\, dx \\ &= \frac{d}{dt} \int_\Omega \dot{\boldsymbol{u}} \cdot \boldsymbol{w}\, dx = \left(\frac{d\boldsymbol{\mathcal{L}}(\boldsymbol{u})}{dt}\right) \cdot \boldsymbol{w} \end{aligned} \tag{16}$$

For the angular momentum $\boldsymbol{\mathcal{D}}(\boldsymbol{u}) = (\boldsymbol{u} \times \dot{\boldsymbol{u}}, 1) \in \mathbb{R}^d$ we have to assume that the forces are central forces, such that $\int_\Omega (\rho \boldsymbol{f} \times \boldsymbol{u})\, dx = 0$ and we take the trial function $\boldsymbol{v} = \boldsymbol{w} \times \boldsymbol{u}$ where $\boldsymbol{w} \in \boldsymbol{H}^1$ is constant. This leads to

$$\begin{aligned} 0 &= \underbrace{\int_\Omega \boldsymbol{\sigma}(\boldsymbol{u}) : \boldsymbol{\epsilon}(\boldsymbol{v})\, dx}_{0} + \int_\Omega \rho \ddot{\boldsymbol{u}} \cdot (\boldsymbol{w} \times \boldsymbol{u})\, dx + \underbrace{\int_\Omega \boldsymbol{w} \cdot (\rho \boldsymbol{f} \times \boldsymbol{u})\, dx}_{0} + \int_{\Gamma_C^S} \boldsymbol{w} \cdot \big[\hat{\boldsymbol{\sigma}}\big(\boldsymbol{u}^S\big) \times \big(\boldsymbol{u}^S - \boldsymbol{u}^M \circ \boldsymbol{\phi}\big)\big]\, dx \\ &= \left(\frac{d\boldsymbol{\mathcal{D}}(\boldsymbol{u})}{dt}\right) \cdot \boldsymbol{w} + \underbrace{\int_{\Gamma_C^S} \boldsymbol{w} \cdot \big[\hat{\boldsymbol{\sigma}}\big(\boldsymbol{u}^S\big) \times \big(\boldsymbol{u}^S - \boldsymbol{u}^M \circ \boldsymbol{\phi}\big)\big]\, dx}_{(*)} \end{aligned} \tag{17}$$

The last term $(*)$ disappears if the contact stresses $\hat{\boldsymbol{\sigma}}(\boldsymbol{u}^S)$ are parallel to $(\boldsymbol{u}^S - \boldsymbol{u}^M \circ \boldsymbol{\phi})$. If the linearized non-penetration condition is used, we cannot expect $\hat{\boldsymbol{\sigma}}(\boldsymbol{u}^S)$ to be parallel to $(\boldsymbol{u}^S - \boldsymbol{u}^M \circ \boldsymbol{\phi})$. As we present the approaches under the unifying assumption of small deformations, we take the linearized non-penetration condition. Therefore, we do not dive in any details concerning the conservation of the angular momentum, whereas the behavior of the energy and the linear momentum plays an important role in the following discussion.

2. Classical Newmark scheme for contact problems

All the algorithms we like to present in this article are based on the classical Newmark scheme. Therefore, we first introduce the classical version of the Newmark scheme with its advantages and disadvantages.

Let $\tau > 0$ denote a discrete time step size and the solution at the discrete time $t^n = t^0 + n \cdot \tau$ is $\boldsymbol{u}^n$. The classical Newmark scheme, which is based on Taylor expansion of the displacements and the velocities, is given by

$$\begin{aligned} \boldsymbol{u}^{n+1} &= \boldsymbol{u}^n + \tau \dot{\boldsymbol{u}}^n + \frac{\tau^2}{2}\big((1-2\beta)\ddot{\boldsymbol{u}}^n + 2\beta \ddot{\boldsymbol{u}}^{n+1}\big) \\ \dot{\boldsymbol{u}}^{n+1} &= \dot{\boldsymbol{u}}^n + \tau\big((1-\gamma)\ddot{\boldsymbol{u}}^n + \gamma \ddot{\boldsymbol{u}}^{n+1}\big). \end{aligned} \tag{18}$$

The parameters γ and 2β can be chosen from the interval $[0,1]$. The special choice $2\beta = \gamma = 1/2$ leads to an algorithm conserving energy, linear momentum and angular momentum [10,27] in the unconstrained case. For this choice of parameters the method is of second order consistency.

In the following we assume $\rho = 1$ and we use the relation between the accelerations and the forces, which is given by Newton's equation of motion $\ddot{\boldsymbol{u}} = -\boldsymbol{F}(\boldsymbol{u}) + \boldsymbol{F}_{\mathrm{con}}(\boldsymbol{u})$, compare (14). We define $\boldsymbol{F}^{1/2}(\boldsymbol{u}^n, \boldsymbol{u}^{n+1}) := \frac{1}{2}\boldsymbol{F}(\boldsymbol{u}^n) + \frac{1}{2}\boldsymbol{F}(\boldsymbol{u}^{n+1})$ and reformulate (18) for $2\beta = \gamma = 1/2$ to

$$\boldsymbol{u}^{n+1} = \boldsymbol{u}^n + \tau \dot{\boldsymbol{u}}^n - \frac{\tau^2}{2}\left(\boldsymbol{F}^{1/2}\big(\boldsymbol{u}^n, \boldsymbol{u}^{n+1}\big) - \frac{1}{2}\boldsymbol{F}_{\mathrm{con}}\big(\boldsymbol{u}^n\big) - \frac{1}{2}\boldsymbol{F}_{\mathrm{con}}\big(\boldsymbol{u}^{n+1}\big)\right) \tag{19}$$

$$\dot{\boldsymbol{u}}^{n+1} = \dot{\boldsymbol{u}}^n - \tau\left(\boldsymbol{F}^{1/2}\big(\boldsymbol{u}^n, \boldsymbol{u}^{n+1}\big) - \frac{1}{2}\boldsymbol{F}_{\mathrm{con}}\big(\boldsymbol{u}^n\big) - \frac{1}{2}\boldsymbol{F}_{\mathrm{con}}\big(\boldsymbol{u}^{n+1}\big)\right). \tag{20}$$

As $\boldsymbol{F}_{\mathrm{con}}(\boldsymbol{u}^{n+1})$ is part of the solution, (19) has to be understood as the variational inclusion

$$\boldsymbol{0} \in \boldsymbol{u}^{n+1} - \boldsymbol{u}^n - \tau \dot{\boldsymbol{u}}^n + \frac{1}{2}\tau^2\left(\boldsymbol{F}^{1/2}\big(\boldsymbol{u}^n, \boldsymbol{u}^{n+1}\big) - \frac{1}{2}\boldsymbol{F}_{\mathrm{con}}\big(\boldsymbol{u}^n\big) + \frac{1}{2}\partial \mathcal{I}_{\mathcal{K}}\big(\boldsymbol{u}^{n+1}\big)\right).$$

This is a slight abuse of notation, that we will employ throughout this article.

The conservation of the linear momentum can be easily verified. For simplicity of presentation we assume $\boldsymbol{f} = \boldsymbol{0}$. We take again a constant trial function $\boldsymbol{w} \in \boldsymbol{H}^1$ and have a look at the change of the linear momentum in two successive time steps.

$$\begin{aligned} \big(\mathcal{L}\big(\boldsymbol{u}^{n+1}\big) - \mathcal{L}\big(\boldsymbol{u}^n\big)\big) \cdot \boldsymbol{w} = &-\tau\left(\frac{1}{2}\int_{\Omega} \boldsymbol{\sigma}\big(\boldsymbol{u}^n\big) : \underbrace{\boldsymbol{\epsilon}(\boldsymbol{w})}_{=0}\, dx + \frac{1}{2}\int_{\Omega} \boldsymbol{\sigma}\big(\boldsymbol{u}^{n+1}\big) : \underbrace{\boldsymbol{\epsilon}(\boldsymbol{w})}_{=0}\, dx\right) \\ &+ \tau\left(\frac{1}{2}\int_{\Gamma_C^S} \sigma_\nu^n \cdot \underbrace{[\boldsymbol{w} \cdot \boldsymbol{\nu}]}_{=0}\, dx + \frac{1}{2}\int_{\Gamma_C^S} \sigma_\nu^{n+1} \cdot \underbrace{[\boldsymbol{w} \cdot \boldsymbol{\nu}]}_{=0}\, dx\right) \end{aligned} \tag{21}$$

But unfortunately, due to the additional contact forces, the desirable energy conserving property of the classical Newmark scheme does not hold for the case of contact. This can be seen by taking the difference of the energy in two successive time steps. Combining Eqs. (19) and (20), we derive

$$\begin{aligned} \mathcal{E}\big(\boldsymbol{u}^{n+1}\big) - \mathcal{E}\big(\boldsymbol{u}^n\big) &= \int_{\Omega}\left(\frac{1}{2}\boldsymbol{F}_{\mathrm{con}}\big(\boldsymbol{u}^n\big) + \frac{1}{2}\boldsymbol{F}_{\mathrm{con}}\big(\boldsymbol{u}^{n+1}\big)\right)\big(\boldsymbol{u}^{n+1} - \boldsymbol{u}^n\big)\, dx \\ &= \int_{\Gamma_C^S}\left(\frac{1}{2}\sigma_\nu^n + \frac{1}{2}\sigma_\nu^{n+1}\right)\big[\big(\boldsymbol{u}^{n+1} - \boldsymbol{u}^n\big) \cdot \boldsymbol{\nu}\big]. \end{aligned} \tag{22}$$

We have no energy conservation in the case of frictionless contact unless $[(\boldsymbol{u}^{n+1} - \boldsymbol{u}^n) \cdot \boldsymbol{\nu}] = 0$ where $(\frac{1}{2}\sigma_\nu^n + \frac{1}{2}\sigma_\nu^{n+1}) \neq 0$ at the contact boundary. This condition can be understood as a discrete persistency condition. But as far as we know there exists no algorithm which is able to fulfill both the non-penetration condition and a kind of persistency condition, ensuring the energy conservation simultaneously.

Until now we analyzed only the time discrete system and figured out that the energy is not conserved. As we already mentioned in the introduction, another disadvantage of the classical Newmark scheme is the occurrence of oscillations at the contact boundary. The causes for these undesirable oscillations can be found in the interaction of the discretization in time and space. Therefore, we have a look at the space–time discrete system. The discretization in space is realized by linear finite elements and the corresponding space is denoted by $\boldsymbol{V}_h$. For two-body contact problems, the information transfer between the two bodies is guaranteed by mortar finite elements [28,29,5]. Here, we employ a discretization where the nodal basis functions μ_p corresponding to the nodes $\boldsymbol{p}$ at the contact boundary on the slave side span the space of relative displacements $\boldsymbol{u}_{\text{rel}} := [\boldsymbol{u}]$, denoted by $\boldsymbol{V}_{h,\text{rel}} := \operatorname{span}\{\mu_p \boldsymbol{e}_1, \dots, \mu_p \boldsymbol{e}_d \ \forall \boldsymbol{p} \in \Gamma_C^S\}$, where $\boldsymbol{e}_1, \dots, \boldsymbol{e}_d$ are the Cartesian basis vectors. In consequence the constraint $[\boldsymbol{u} \cdot \boldsymbol{\nu}] \leqslant g$ as well as the contact force are localized on the slave side. In other words $\boldsymbol{V}_h = \boldsymbol{V}_{h,\text{rel}} \oplus \boldsymbol{V}_{h,[0]}$, where $\boldsymbol{V}_{h,[0]} := \{\boldsymbol{v} \in \boldsymbol{V}_h \mid [\boldsymbol{v}(\boldsymbol{p})] = 0 \ \forall \boldsymbol{p} \in \Gamma_C^S\}$. Remark that in the case of a one body contact problem, the relative displacement is the displacement itself, which means that $\boldsymbol{u}_{\text{rel}} := \boldsymbol{u}$. We denote with $\boldsymbol{M}$ the mass matrix. Then the space-discrete first equation of the classical Newmark scheme in the case of contact (19) reads as

$$\boldsymbol{M}\begin{pmatrix} \boldsymbol{u}^{n+1} \\ \boldsymbol{u}_{\text{rel}}^{n+1} \end{pmatrix} = \boldsymbol{M}\begin{pmatrix} \boldsymbol{u}^{n} + \tau \dot{\boldsymbol{u}}^{n} \\ \boxed{\boldsymbol{u}_{\text{rel}}^{n} + \tau \dot{\boldsymbol{u}}_{\text{rel}}^{n}} \end{pmatrix} - \frac{\tau^2}{4}\boldsymbol{M}\underbrace{\big((\boldsymbol{F} - \boldsymbol{F}_{\text{con}})(\boldsymbol{u}^n) + (\boldsymbol{F} - \boldsymbol{F}_{\text{con}})(\boldsymbol{u}^{n+1})\big)}_{\text{expected equilibration}}. \tag{23}$$

The term $\boldsymbol{u}_{\text{rel}}^n + \tau \dot{\boldsymbol{u}}_{\text{rel}}^n$ in the box is the crucial part. In the continuous case in oder to ensure the non-penetration condition the contact forces $\boldsymbol{F}_{\text{con}}$ equilibrate $\boldsymbol{F}$ at the contact boundary in normal direction. Therefore, we would expect in the discrete version $(\boldsymbol{F} - \boldsymbol{F}_{\text{con}})(\boldsymbol{u}^n) \cdot \boldsymbol{\nu} + (\boldsymbol{F} - \boldsymbol{F}_{\text{con}})(\boldsymbol{u}^{n+1}) \cdot \boldsymbol{\nu} = 0$ at the contact boundary. But in the space-discrete case we have entries in the mass matrix at the contact boundary although in the continuous case the boundary has measure zero. Thus, the constraining force $\boldsymbol{F}_{\text{con}}$ to the non-penetration condition also reacts to $\boldsymbol{M}(\boldsymbol{u}_{\text{rel}}^n + \tau \dot{\boldsymbol{u}}_{\text{rel}}^n)$ if this part causes penetration of the two bodies. The problem is that this contribution to $\boldsymbol{F}_{\text{con}}$ has no realistic physical meaning and it evokes the oscillations in the contact forces as one can see from a simple combination of the two lines of the Newmark scheme under the assumption of $\boldsymbol{u}_{\text{rel}}^{n+1} \cdot \boldsymbol{\nu} = \boldsymbol{u}_{\text{rel}}^{n} \cdot \boldsymbol{\nu}$.

$$\begin{aligned} \dot{\boldsymbol{u}}_{\text{rel}}^{n+1} \cdot \boldsymbol{\nu} &= \dot{\boldsymbol{u}}_{\text{rel}}^{n} \cdot \boldsymbol{\nu} - \tau\left(\boldsymbol{F}_{\text{rel}}^{1/2}\big(\boldsymbol{u}^n, \boldsymbol{u}^{n+1}\big) - \frac{1}{2}\boldsymbol{F}_{\text{con}}\big(\boldsymbol{u}^n\big) - \frac{1}{2}\boldsymbol{F}_{\text{con}}\big(\boldsymbol{u}^{n+1}\big)\right) \cdot \boldsymbol{\nu} \\ &= \dot{\boldsymbol{u}}_{\text{rel}}^{n} \cdot \boldsymbol{\nu} + \tau\left(\frac{2}{\tau^2}\big(\boldsymbol{u}_{\text{rel}}^{n+1} - \big(\boldsymbol{u}_{\text{rel}}^{n} + \tau \dot{\boldsymbol{u}}_{\text{rel}}^{n}\big)\big)\right) \cdot \boldsymbol{\nu} \\ &= -\dot{\boldsymbol{u}}_{\text{rel}}^{n} \cdot \boldsymbol{\nu} \end{aligned} \tag{24}$$

This zigzagging in the velocities $\dot{\boldsymbol{u}}_{\text{rel}}^{n+1} \cdot \boldsymbol{\nu}$ gets translated to the contact forces by $(\boldsymbol{u}_{\text{rel}}^n + \tau \dot{\boldsymbol{u}}_{\text{rel}}^n) \cdot \boldsymbol{\nu}$.

3. Presentation of selected algorithms for dynamic contact

In the following subsections we present the algorithms, mentioned in the introduction, in a unifying framework. As far as possible we use the same notation. Further we assume linear elastic materials, allowing for a linearized non-penetration condition.

3.1. Importance of the persistency condition — Algorithm of Laursen and Chawla

In [23] Laursen and Chawla present an algorithm which conserves energy, linear momentum and angular momentum. They use the time discretization scheme

$$\begin{aligned} \boldsymbol{u}^{n+1} &= \boldsymbol{u}^n + \tau \dot{\boldsymbol{u}}^n + \alpha\tau^2\big(\alpha \ddot{\boldsymbol{u}}^{n+1} + (1-\alpha)\ddot{\boldsymbol{u}}^n\big) \\ \dot{\boldsymbol{u}}^{n+1} &= \dot{\boldsymbol{u}}^n + \tau\big(\alpha \ddot{\boldsymbol{u}}^{n+1} + (1-\alpha)\ddot{\boldsymbol{u}}^n\big) \end{aligned}$$

proposed in [27] with $\alpha = 1/2$. This corresponds to the classical Newmark scheme with the parameters $2\beta = \gamma = \frac{1}{2}$ which we discussed in the last section.

Laursen and Chawla use their algorithm for the computation of large deformation. Therefore, they do not use a linearized non-penetration condition. With the same arguments as in (16), respectively (21) and (17), one can proof the conservation of the linear and angular momentum. As we know from (22), the classical Newmark scheme does not conserve the energy in the case of contact. A discrete kind of the persistency condition (15) has to be fulfilled, ensuring $[(\boldsymbol{u}^{n+1} - \boldsymbol{u}^n) \cdot \boldsymbol{\nu}] = 0$ if contact forces occur, compare (22). Therefore, Laursen and Chawla introduce the following constraints

$$\lambda_\nu \leqslant 0 \tag{25}$$

$$\tilde{g}_\nu\big(\boldsymbol{u}^n, \boldsymbol{u}^{n+1}\big) \leqslant 0 \tag{26}$$

$$\lambda_\nu \cdot \tilde{g}_\nu\big(\boldsymbol{u}^n, \boldsymbol{u}^{n+1}\big) = 0 \tag{27}$$

where

$$\tilde{g}_\nu\big(\boldsymbol{u}^n, \boldsymbol{u}^{n+1}\big) = \frac{1}{\tau} \cdot \big[\big(\boldsymbol{u}^{n+1} - \boldsymbol{u}^n\big) \cdot \boldsymbol{\nu}\big]$$

which is called the algorithmic gap rate. The expression (27) is a so-called algorithmic persistency condition.

In each time step $n+1$ the algorithm demands to check for each point if penetration or contact occurred in the previous time step. At the points where penetration or contact occurred in the previous time step, the constraint (26) has to be fulfilled, which means that the Lagrange multiplier λ_ν acts as a contact force to avoid further penetration of the two bodies. At the points where no penetration or contact occurred in the last time step, no constraints have to be fulfilled and therefore $\lambda_\nu = 0$ at this points.

In order to reformulate the algorithm proposed by Laursen and Chawla in our setting, let $\boldsymbol{F}$ be defined as in Section 1 and $(\boldsymbol{F}_{\mathrm{con}}(\boldsymbol{u}^n, \boldsymbol{u}^{n+1}), \boldsymbol{\nu})_{L^2(\Omega)} := (\lambda_\nu \boldsymbol{\nu}, \boldsymbol{\nu})_{L^2(\Gamma_C)}$. Then we get the compact form of the algorithm.

Algorithm 1.

$$\begin{aligned}
\boldsymbol{u}^{n+1} &= \boldsymbol{u}^n + \tau \dot{\boldsymbol{u}}^n - \frac{\tau^2}{2}\big(\boldsymbol{F}^{1/2}\big(\boldsymbol{u}^n, \boldsymbol{u}^{n+1}\big) - \boldsymbol{F}_{\mathrm{con}}\big(\boldsymbol{u}^n, \boldsymbol{u}^{n+1}\big)\big)\\
\dot{\boldsymbol{u}}^{n+1} &= \dot{\boldsymbol{u}}^n - \tau\big(\boldsymbol{F}^{1/2}\big(\boldsymbol{u}^n, \boldsymbol{u}^{n+1}\big) - \boldsymbol{F}_{\mathrm{con}}\big(\boldsymbol{u}^n, \boldsymbol{u}^{n+1}\big)\big)
\end{aligned}$$

The authors of [23] use penalty and augmented Lagrangian methods to solve the arising variational inequalities.

The extension of this algorithm to frictional contact can be found in [2]. Whenever the constraint $[(\boldsymbol{u}^{n+1} - \boldsymbol{u}^n) \cdot \boldsymbol{\nu}] \leqslant 0$ is active at a point $\boldsymbol{x}$, frictional effects are considered in this point $\boldsymbol{x}$. Similar to the definition of the algorithmic gap rate in normal direction, an algorithmic gap rate in tangential direction is defined

$$\tilde{\boldsymbol{g}}_T\big(\boldsymbol{u}^n, \boldsymbol{u}^{n+1}\big) := \frac{1}{\tau}\big[\big(\boldsymbol{u}^{n+1} - \boldsymbol{u}^n\big)_T\big].$$

In a first step, it has to be checked if perfect stick, $\tilde{\boldsymbol{g}}_T(\boldsymbol{x}) = \boldsymbol{0}$ holds. In this case, the solution must be $\boldsymbol{u}_T^{n+1}(\boldsymbol{x}) = \boldsymbol{u}_T^n(\boldsymbol{x})$ and the normal and tangential stresses $\lambda_\nu(\boldsymbol{x})$ and $\boldsymbol{\lambda}_T^{\mathrm{trial}}(\boldsymbol{x})$ can be computed. Then it can be checked if the friction law for a sticky node $\|\boldsymbol{\lambda}_T^{\mathrm{trial}}(\boldsymbol{x})\| \leqslant -\mathcal{F}|\lambda_\nu(\boldsymbol{x})|$ holds. Otherwise, if the friction law for a sticky node is not fulfilled, the node must be a sliding node. Therefore, a tangential stress $\boldsymbol{\lambda}_T(\boldsymbol{x}) := -\mathcal{F}|\lambda_\nu(\boldsymbol{x})|\frac{\boldsymbol{\lambda}_T^{\mathrm{trial}}(\boldsymbol{x})}{\|\boldsymbol{\lambda}_T^{\mathrm{trial}}(\boldsymbol{x})\|}$ is computed and for the tangential displacement the authors of [2] use a return map, see, e.g. [30].

3.2. Discrete velocity at the contact boundary — Algorithm of Laursen and Love

Laursen and Love provide a method in [24] which assures the non-penetration condition as well as the conservation of energy in the fully discrete setting. This algorithm is also used for the computation of large deformation. In case no kind of penalty method is used to solve the arising variational formulation, the method allows for a pure implicit treatment of the contact forces, which are the constraining forces to the non-penetration condition. But we have to mention that the authors of [24] use a penalty or an augmented Lagrangian formulation for which the contact forces depend on $\boldsymbol{u}^{n+1}$ and $\boldsymbol{u}^n$. In the second step of the Newmark method, in which the velocities are updated, they add a discrete contact-related correction denoted by $\dot{\boldsymbol{u}}_{\mathrm{con}}^{n+1}$ in order to enforce the conservation of energy.

Algorithm 2.

$$\begin{aligned}
\boldsymbol{u}^{n+1} &= \boldsymbol{u}^n + \tau \dot{\boldsymbol{u}}^n - \frac{1}{2}\tau^2\big(\boldsymbol{F}^{1/2}\big(\boldsymbol{u}^n, \boldsymbol{u}^{n+1}\big) - \boldsymbol{F}_{\mathrm{con}}\big(\boldsymbol{u}^{n+1}\big)\big)\\
\dot{\boldsymbol{u}}^{n+1} &= \dot{\boldsymbol{u}}^n - \tau\big(\boldsymbol{F}^{1/2}\big(\boldsymbol{u}^n, \boldsymbol{u}^{n+1}\big) - \boldsymbol{F}_{\mathrm{con}}\big(\boldsymbol{u}^{n+1}\big)\big) + \dot{\boldsymbol{u}}_{\mathrm{con}}^{n+1}
\end{aligned}$$

Adding a discrete contact-related correction $\dot{\boldsymbol{u}}_{\mathrm{con}}^{n+1}$ to the velocities, in order to enforce the conservation of energy, may disturb the natural properties of the classical Newmark scheme, namely the conservation of linear and angular momentum. Therefore, not only the energy conservation but also the conservation of linear and angular momentum have to be taken into account in the computation of $\dot{\boldsymbol{u}}_{\mathrm{con}}^{n+1}$. In order to compute this discrete contact-related correction algebraically, so-called contact impulses, which in analogy to the contact stresses have opposite sign on the two contacting boundaries, are introduced. This special ansatz leads to a sum of coupled quadratic equations for $\dot{\boldsymbol{u}}_{\mathrm{con}}^{n+1}$ which may have an infinite number of solutions. Under several assumptions a physically reasonable solution is selected in [24].

In [25] this algorithm was extended to frictional contact. Similar to [2] the frictional effects are measured in terms of the algorithmic gap rate $[(\boldsymbol{u}^{n+1} - \boldsymbol{u}^n)_T]$ and are computed via an augmented Lagrangian method in the first step of the Newmark scheme. The computation of the contact-related correction $\dot{\boldsymbol{u}}_{\mathrm{con}}^{n+1}$ of the velocities ensures that the algorithmic energy loss represents exactly the amount of energy dissipated by friction.

3.3. Removing the discrete mass from the contact boundary — Algorithm of Khenous, Laborde and Renard

In all the previously presented algorithms the boundary gets assigned to a mass due to the discretization in space although in the continuous case the boundary has measure zero. The interplay of the discrete mass at the contact boundary and the time discretization evokes artificial contact forces as already explained in Section 2, see for example equation (23). Khenous et al. [13,14,12] introduce a mass redistribution method, in which mass from the contact boundary is moved to the interior. Thereby the entire mass, the moment of inertia and the center of gravity remain the same. To keep the complexity as low as possible, the zero entries of the standard mass matrix are kept. The redistributed mass matrix $\tilde{\boldsymbol{M}}$ is computed as minimization problem of the distance to the standard mass matrix $\boldsymbol{M}$ under the constraints mentioned above. The method is proposed for one-body contact problems but it is easily extendable to two-body contact problems.

In [13,14,12] the discretization takes place first in space second in time. After discretizing in space the hyperbolic variational inequality (11) and applying the mass redistribution, they get the following variational inequality, which is a coupled system in the variables belonging to the parts with mass $(\cdot)_m$ or without mass $(\cdot)_{\not m}$.

$$\begin{pmatrix} \tilde{\boldsymbol{M}} & \boldsymbol{0} \\ \boldsymbol{0} & \boldsymbol{0} \end{pmatrix} \begin{pmatrix} \ddot{\boldsymbol{u}}_m \\ \ddot{\boldsymbol{u}}_{\not m} \end{pmatrix} + \begin{pmatrix} \boldsymbol{A}_{m,m} & \boldsymbol{A}_{\not m,m}^T \\ \boldsymbol{A}_{\not m,m} & \boldsymbol{A}_{\not m,\not m} \end{pmatrix} \begin{pmatrix} \boldsymbol{u}_m \\ \boldsymbol{u}_{\not m} \end{pmatrix} = \begin{pmatrix} \boldsymbol{f}_m \\ \boldsymbol{f}_{\not m} \end{pmatrix} + \sum_{p \in \Gamma_C^S} \lambda_{p,\nu} \begin{pmatrix} \boldsymbol{0} \\ \boldsymbol{\nu}(p) \end{pmatrix} \tag{28}$$

Here $\lambda_{p,\nu}$ corresponds to the discrete contact stress at a node $\boldsymbol{p} \in \Gamma_C^S$. The initial values are

$$\boldsymbol{u}(\boldsymbol{x}, 0) = \boldsymbol{u}^0$$
$$\dot{\boldsymbol{u}}(\boldsymbol{x}, 0) = \dot{\boldsymbol{u}}^0$$

and the constraints

$$\boldsymbol{u}(\boldsymbol{p}) \cdot \boldsymbol{\nu}(\boldsymbol{p}) \leqslant g(\boldsymbol{p})$$
$$\lambda_{p,\nu} \leqslant 0$$
$$\lambda_{p,\nu} \cdot \boldsymbol{u}(\boldsymbol{p}) \cdot \boldsymbol{\nu}(\boldsymbol{p}) = 0$$

hold for each time step and all nodes $\boldsymbol{p} \in \Gamma_C^S$. This means that the non-penetration condition is fulfilled. Now the system of equations is divided as follows:

$$\begin{aligned} \tilde{\boldsymbol{M}} \ddot{\boldsymbol{u}}_m + \boldsymbol{A}_{m,m} \boldsymbol{u}_m &= \boldsymbol{f}_m - \boldsymbol{A}_{\not m,m}^T \boldsymbol{u}_{\not m} \\ \boldsymbol{A}_{\not m,m} \boldsymbol{u}_m + \boldsymbol{A}_{\not m,\not m} \boldsymbol{u}_{\not m} &= \boldsymbol{f}_{\not m} + \sum_{p \in \Gamma_C^S} \lambda_{p,\nu} \cdot \boldsymbol{\nu}(\boldsymbol{p}). \end{aligned} \tag{29}$$

The second equation is a variational inequality

$$a\big(\boldsymbol{u}_{\not m}, (\boldsymbol{v} - \boldsymbol{u})_{\not m}\big) \geqslant l_{u_m}\big((\boldsymbol{v} - \boldsymbol{u})_{\not m}\big)$$

with

$$a(\boldsymbol{u}_{\not m}, \boldsymbol{v}_{\not m}) = \boldsymbol{v}_{\not m}^T \boldsymbol{A}_{\not m,\not m} \boldsymbol{u}_{\not m}$$
$$l_{u_m}(\boldsymbol{v}_{\not m}) = \boldsymbol{v}_{\not m}^T \boldsymbol{f}_{\not m} - \boldsymbol{v}_{\not m}^T \boldsymbol{A}_{\not m,m} \boldsymbol{u}_m.$$

It is proven in [13] that there exists one and only one Lipschitz continuous function $t \mapsto (\boldsymbol{u}, \{\lambda_{\nu,p}(t)\}_p)$ satisfying the system (29) with the contact constraints and the initial conditions under the assumption that $\boldsymbol{f}$ is Lipschitz continuous on $[0, T]$.

For the discretization in time the authors of [14] test the Crank–Nicholson method as well as the Newmark method with the parameters $\beta = \gamma = 1/2$. Independently of the method, the redistributed mass matrix reduces the oscillations in the contact forces as well as the changes in the total energy. The Newmark scheme with $\gamma = \beta = 1/2$:

$$\begin{aligned} \boldsymbol{u}^{n+1} &= \boldsymbol{u}^n + \tau \dot{\boldsymbol{u}} + \frac{\tau^2}{2} \ddot{\boldsymbol{u}}^{n+1} \\ \dot{\boldsymbol{u}}^{n+1} &= \dot{\boldsymbol{u}}^n + \frac{\tau}{2}\big(\ddot{\boldsymbol{u}}^n + \ddot{\boldsymbol{u}}^{n+1}\big) \end{aligned} \tag{30}$$

takes the accelerations purely implicitly in the first step. Combining (30) and (28) and assuming that we have no volume forces $\boldsymbol{f} = \boldsymbol{0}$ leads to the following equation for the computation of the displacements.

Algorithm 3.

$$\begin{pmatrix} \tilde{\boldsymbol{M}} + \frac{\tau^2}{2}\boldsymbol{A}_{m,m} & \frac{\tau^2}{2}\boldsymbol{A}_{\dot{m},m}^T \\ \frac{\tau^2}{2}\boldsymbol{A}_{\dot{m},m} & \frac{\tau^2}{2}\boldsymbol{A}_{\dot{m},\dot{m}} \end{pmatrix} \begin{pmatrix} \boldsymbol{u}_m^{n+1} \\ \boldsymbol{u}_{\dot{m}}^{n+1} \end{pmatrix} = \begin{pmatrix} \tilde{\boldsymbol{M}}(\boldsymbol{u}_m^n + \tau \dot{\boldsymbol{u}}_m^n) \\ \boldsymbol{0} \end{pmatrix} + \underbrace{\frac{\tau^2}{2} \sum_{p \in \Gamma_C^S} \lambda_{p,\nu} \begin{pmatrix} \boldsymbol{0} \\ \boldsymbol{\nu}(\boldsymbol{p}) \end{pmatrix}}_{=\boldsymbol{M}\boldsymbol{F}_{\mathrm{con}}(\boldsymbol{u}^{n+1})}$$

3.4. Mass redistribution with less computational costs — Algorithm of Hager, Hüeber and Wohlmuth

Unfortunately, the algorithm of Khenous et al. requires extra computational costs, as the redistribution of the mass matrix necessitates a minimization problem, in the dimension of the mass matrix, under constraints. Hager et al. [9] circumvent this problem by using special quadrature formulas on so-called macro-elements to compute the mass redistribution.

In order to explain the macro-elements, we assume a mesh $\mathcal{T}_h$ of the domain Ω to be given. The small strip of all elements $T_h \in \mathcal{T}_h$ which have an edge or a face on $\bar{\Gamma}_C$ is denoted by Ω_C and the remaining elements of $\mathcal{T}_h$ constitute Ω_I. Each macro-element $T_H \in \mathcal{T}_H$ is either an element $T_h \in \Omega_I$ or a union of an element $T_h \in \Omega_I$ with elements $T_h \in \Omega_C$. The quadrature formula used on the macro-elements has no quadrature points placed in $\Omega_C \cup \bar{\Gamma}_C$, which directly implies that the new mass matrix $\tilde{\boldsymbol{M}}$ has no entries for basis functions at the contact boundary. Furthermore the quadrature formula is chosen such that it is exact on each macro-element $T_H \in \mathcal{T}_H$ for all quadratic functions on T_H. Due to these properties of the quadrature formula, the redistributed mass matrix $\tilde{\boldsymbol{M}}$ leads to the same total mass, center of gravity and moment of inertia as given by the standard mass matrix $\boldsymbol{M}$.

As we already know from the algorithm of Khenous et al., the modified mass matrix reduces the oscillations in the contact stresses. Further the modified mass matrix is embedded in the algorithm of Laursen and Chawla which means that the discrete persistency condition is enforced instead of the non-penetration condition. Therefore, the whole energy $\mathcal{E} = \mathcal{E}_{\mathrm{pot}} + \mathcal{E}_{\mathrm{kin}}$ is conserved if the kinetic energy $\mathcal{E}_{\mathrm{kin}} = \frac{1}{2}\dot{\boldsymbol{u}}\tilde{\boldsymbol{M}}\dot{\boldsymbol{u}}$ is computed with the redistributed mass matrix. That leads to the following algorithm:

Algorithm 4.

$$\begin{pmatrix} \tilde{\boldsymbol{M}} + \frac{\tau^2}{4}\boldsymbol{A}_{m,m} & \frac{\tau^2}{4}\boldsymbol{A}_{\dot{m},m}^T \\ \frac{\tau^2}{4}\boldsymbol{A}_{\dot{m},m} & \frac{\tau^2}{4}\boldsymbol{A}_{\dot{m},\dot{m}} \end{pmatrix} \begin{pmatrix} \boldsymbol{u}_m^{n+1} \\ \boldsymbol{u}_{\dot{m}}^{n+1} \end{pmatrix}$$
$$= \begin{pmatrix} \tilde{\boldsymbol{M}}(\boldsymbol{u}_m^n + \tau \dot{\boldsymbol{u}}_m^n) \\ \boldsymbol{0} \end{pmatrix} - \begin{pmatrix} \frac{\tau^2}{4}\boldsymbol{A}_{m,m} & \frac{\tau^2}{4}\boldsymbol{A}_{\dot{m},m}^T \\ \frac{\tau^2}{4}\boldsymbol{A}_{\dot{m},m} & \frac{\tau^2}{4}\boldsymbol{A}_{\dot{m},\dot{m}} \end{pmatrix} \begin{pmatrix} \boldsymbol{u}_m^n \\ \boldsymbol{u}_{\dot{m}}^n \end{pmatrix} + \underbrace{\frac{\tau^2}{2} \sum_{p \in \Gamma_C^S} \lambda_{p,\nu} \begin{pmatrix} \boldsymbol{0} \\ \boldsymbol{\nu}(\boldsymbol{p}) \end{pmatrix}}_{=\boldsymbol{M}\boldsymbol{F}_{\mathrm{con}}(\boldsymbol{u}^{n+1})}$$

$$\dot{\boldsymbol{u}}^{n+1} = -\dot{\boldsymbol{u}}^n + \frac{2}{\tau}\left(\boldsymbol{u}^{n+1} - \boldsymbol{u}^n\right)$$

where $(\boldsymbol{F}_{\mathrm{con}}(\boldsymbol{u}^n, \boldsymbol{u}^{n+1}), \boldsymbol{v})_{L^2(\Omega)} := (\lambda_\nu \boldsymbol{v}, \boldsymbol{v})_{L^2(\Gamma_C)}$ with λ_ν Lagrange multiplier to the constraints (25)–(27) in each point, identified as contact point in the previous time step or $\lambda_\nu = 0$ for non-contact points.

This algorithm is originally designed for frictional contact problems. As in [2], the frictional effects influence the algorithmic tangential gap rate $[(\boldsymbol{u}^{n+1} - \boldsymbol{u}^n)_T]$ instead of the velocity $[\dot{\boldsymbol{u}}_T]$. The modified friction law is

$$\begin{aligned} \left[\boldsymbol{u}_T^{n+1} - \boldsymbol{u}_T^n\right] = \boldsymbol{0} \quad &\Rightarrow \quad \left\|\boldsymbol{\lambda}_T\left(\boldsymbol{u}^{n+1}\right)\right\| \leqslant \mathcal{F}|\lambda_\nu| \\ \left[\boldsymbol{u}_T^{n+1} - \boldsymbol{u}_T^n\right] \neq \boldsymbol{0} \quad &\Rightarrow \quad \boldsymbol{\lambda}_T\left(\boldsymbol{u}^{n+1}\right) = -\mathcal{F}|\lambda_\nu| \frac{[\boldsymbol{u}_T^{n+1} - \boldsymbol{u}_T^n]}{\|[\boldsymbol{u}_T^{n+1} - \boldsymbol{u}_T^n]\|}. \end{aligned} \tag{31}$$

For the numerical resolution of the contact and frictional constraints, a primal–dual active set strategy is used in [9].

3.5. Prediction of the contact boundary — Algorithm of Deuflhard, Krause and Ertel

In [4] Deuflhard et al. present a contact-stabilized Newmark scheme whose particular feature is the stable behavior of the contact forces. A special predictor step prevents the unphysical part of the contact forces. Additionally, the purely implicit treatment of the contact forces as first introduced in [11] avoids energy blow-ups.

The Newmark scheme with purely implicit treatment of the contact forces is given by the following algorithm which we call contact–implicit Newmark scheme.

Algorithm 5 *(Contact-implicit Newmark scheme).*

$$\boldsymbol{u}_{\text{pred}}^{n+1} = \boldsymbol{u}^n + \tau \dot{\boldsymbol{u}}^n \tag{32}$$

$$\boldsymbol{u}^{n+1} = \boldsymbol{u}_{\text{pred}}^{n+1} - \frac{\tau^2}{2}\big(\boldsymbol{F}^{1/2}\big(\boldsymbol{u}^n, \boldsymbol{u}^{n+1}\big) - \boldsymbol{F}_{\text{con}}\big(\boldsymbol{u}^{n+1}\big)\big) \tag{33}$$

$$\dot{\boldsymbol{u}}^{n+1} = \dot{\boldsymbol{u}}^n - \tau\big(\boldsymbol{F}^{1/2}\big(\boldsymbol{u}^n, \boldsymbol{u}^{n+1}\big) - \boldsymbol{F}_{\text{con}}\big(\boldsymbol{u}^{n+1}\big)\big) \tag{34}$$

The change of the total energy between two successive time steps is

$$\mathcal{E}\big(\boldsymbol{u}^{n+1}\big) - \mathcal{E}\big(\boldsymbol{u}^n\big) = \int_\Omega \boldsymbol{F}_{\text{con}}\big(\boldsymbol{u}^{n+1}\big)\big(\boldsymbol{u}^{n+1} - \boldsymbol{u}^n\big)\,dx$$

see [4]. From the variational inequality follows that $(\boldsymbol{F}_{\text{con}}(\boldsymbol{u}^{n+1}), \boldsymbol{u}^{n+1} - \boldsymbol{v}) \leqslant 0$ for all $\boldsymbol{v} \in \mathcal{K}$. As $\boldsymbol{u}^n \in \mathcal{K}$ we have $\mathcal{E}(\boldsymbol{u}^{n+1}) - \mathcal{E}(\boldsymbol{u}^n) \leqslant 0$ which means that the method is dissipative and especially energy blow-ups will never occur.

Unfortunately, the implicit treatment of the contact forces as in [11] does not prevent oscillations at the contact boundary. As already explained in Section 2, the main reason for this can be found in an unwanted interaction of space and time discretization.

In order to overcome this deficiency, step (32) is replaced by the variational inclusion

$$\boldsymbol{0} \in \boldsymbol{u}_{\text{pred}}^{n+1} - \big(\boldsymbol{u}^n + \tau \dot{\boldsymbol{u}}^n\big) + \partial \mathcal{I}_{\mathcal{K}}\big(\boldsymbol{u}_{\text{pred}}^{n+1}\big) \tag{35}$$

which is called predictor step. This variational inclusion requires the evaluation of the normal trace of an $\boldsymbol{L}^2$-function which is not possible in general. But corresponding to the fact that the discrete boundary gets assigned to a mass, finite element functions have boundary values. The solution $\boldsymbol{u}_{\text{pred}}^{n+1}$ of (35) is the same as the $\boldsymbol{L}^2$-projection of the standard predictor (32) onto the admissible set $\mathcal{K}$. As $\boldsymbol{u}_{\text{pred}}^{n+1}$ of (35) is already contained in the admissible set $\mathcal{K}$, one can imagine that $\boldsymbol{u}_{\text{pred,rel}}^{n+1} \cdot \boldsymbol{\nu}$ predicts $\boldsymbol{u}_{\text{rel}}^{n+1} \cdot \boldsymbol{\nu}$ at the contact boundary. If $\boldsymbol{u}_{\text{pred,rel}}^{n+1} \cdot \boldsymbol{\nu} = \boldsymbol{u}_{\text{rel}}^{n+1} \cdot \boldsymbol{\nu}$ at the contact boundary, $\boldsymbol{F}_{\text{con}}(\boldsymbol{u}^{n+1}) \cdot \boldsymbol{\nu}$ equilibrates $\boldsymbol{F}^{1/2}(\boldsymbol{u}^n, \boldsymbol{u}^{n+1}) \cdot \boldsymbol{\nu}$ in (33) which corresponds to Newton's Axiom of the equilibrium of forces. The artificial part of the contact forces is removed, compare the discussion to Eq. (23). Further, the force equilibrium directly implies $\dot{\boldsymbol{u}}_{\text{rel}}^n \cdot \boldsymbol{\nu} = \dot{\boldsymbol{u}}_{\text{rel}}^{n+1} \cdot \boldsymbol{\nu}$ which means that there is no zigzagging as in the classical Newmark scheme.

We define $\boldsymbol{G}_{\text{con}}(\boldsymbol{u}_{\text{pred}}^{n+1}) \in \partial \mathcal{I}_{\mathcal{K}}(\boldsymbol{u}_{\text{pred}}^{n+1})$ as the element of $\partial \mathcal{I}_{\mathcal{K}}(\boldsymbol{u}_{\text{pred}}^{n+1})$ fulfilling $(\boldsymbol{G}_{\text{con}}(\boldsymbol{u}_{\text{pred}}^{n+1}), \boldsymbol{v}) = (\boldsymbol{u}^n + \tau \dot{\boldsymbol{u}}^n - \boldsymbol{u}_{\text{pred}}^{n+1}, \boldsymbol{v})$. Note that the quantity $\boldsymbol{G}_{\text{con}}(\boldsymbol{u}_{\text{pred}}^{n+1})$ corresponds to displacements. The artificial part of the contact forces removed in the predictor step is given by $\tilde{\boldsymbol{G}}_{\text{con}} := \frac{2}{\tau^2}\boldsymbol{G}_{\text{con}}$. This notation directly leads us to the following formulation of the contact-stabilized Newmark scheme.

Algorithm 6 *(Contact-stabilized Newmark scheme).*

$$\boldsymbol{u}_{\text{pred}}^{n+1} = \boldsymbol{u}^n + \tau \dot{\boldsymbol{u}}^n - \boldsymbol{G}_{\text{con}}\big(\boldsymbol{u}_{\text{pred}}^{n+1}\big) \tag{36}$$

$$\boldsymbol{u}^{n+1} = \boldsymbol{u}_{\text{pred}}^{n+1} - \frac{1}{2}\tau^2\big(\boldsymbol{F}^{1/2}\big(\boldsymbol{u}^n, \boldsymbol{u}^{n+1}\big) - \boldsymbol{F}_{\text{con}}\big(\boldsymbol{u}^{n+1}\big)\big) \tag{37}$$

$$\dot{\boldsymbol{u}}^{n+1} = \dot{\boldsymbol{u}}^n - \tau\big(\boldsymbol{F}^{1/2}\big(\boldsymbol{u}^n, \boldsymbol{u}^{n+1}\big) - \boldsymbol{F}_{\text{con}}\big(\boldsymbol{u}^{n+1}\big)\big) \tag{38}$$

Here the change in the total energy between two successive time steps is

$$\mathcal{E}\big(\boldsymbol{u}^{n+1}\big) - \mathcal{E}\big(\boldsymbol{u}^n\big) = \underbrace{\int_\Omega \boldsymbol{F}_{\text{con}}\big(\boldsymbol{u}^{n+1}\big)\big(\boldsymbol{u}^{n+1} - \boldsymbol{u}^n\big)\,dx}_{\leqslant 0} + \frac{2}{\tau^2}\int_\Omega \boldsymbol{G}_{\text{con}}\big(\boldsymbol{u}_{\text{pred}}^{n+1}\big)\big(\boldsymbol{u}^{n+1} - \boldsymbol{u}_{\text{pred}}^{n+1}\big)\,dx \tag{39}$$

see [4]. From the variational inequality of the predictor step it follows that $(\boldsymbol{G}_{\text{con}}(\boldsymbol{u}_{\text{pred}}^{n+1}), \boldsymbol{v} - \boldsymbol{u}_{\text{pred}}^{n+1}) \leqslant 0$ for all $\boldsymbol{v} \in \mathcal{K}$. Therewith the algorithm is dissipative. Moreover the algorithm conserves the linear momentum.

In [21] the contact-stabilized Newmark method is extended to the case of friction. We use a time-discretized friction law

$$\begin{aligned}
\big[\boldsymbol{u}_T^{n+1} - \boldsymbol{u}_T^n\big] = \boldsymbol{0} \quad &\Rightarrow \quad \big\|\boldsymbol{\sigma}_T\big(\boldsymbol{u}^{n+1}\big)\big\| \leqslant \mathcal{F}|\sigma_\nu| \\
\big[\boldsymbol{u}_T^{n+1} - \boldsymbol{u}_T^n\big] \neq \boldsymbol{0} \quad &\Rightarrow \quad \boldsymbol{\sigma}_T\big(\boldsymbol{u}^{n+1}\big) = -\mathcal{F}|\sigma_\nu|\frac{[\boldsymbol{u}_T^{n+1} - \boldsymbol{u}_T^n]}{\|[\boldsymbol{u}_T^{n+1} - \boldsymbol{u}_T^n]\|}
\end{aligned} \tag{40}$$

which coincides with the friction law used in [9]. Our motivation for this time-discretized friction law is the implicit treatment of the frictional forces in the context of the Newmark scheme. The computation of the displacements requires

the current forces but in the case of friction the forces depend on the current velocities (10) which are not yet known, because they are updated in the second step, based on the actual displacements. Therefore, the time-discretized friction law with the dependency on the displacements instead of the velocities allows for an implicit treatment of the frictional forces. Let $(\boldsymbol{F}_{\mathrm{fri}},\cdot)_{L^2(\Omega)} := (\boldsymbol{\sigma}_T,\cdot)_{L^2(\Gamma_C)}$ be the frictional forces, the reaction to the friction law, then we get the following time-discretization:

Algorithm 7 *(Contact-stabilized Newmark scheme for frictional contact).*

$$\boldsymbol{u}_{\mathrm{pred}}^{n+1} = \boldsymbol{u}^n + \tau\dot{\boldsymbol{u}}^n - \boldsymbol{G}_{\mathrm{con}}\big(\boldsymbol{u}_{\mathrm{pred}}^{n+1}\big) \tag{41}$$

$$\boldsymbol{u}^{n+1} = \boldsymbol{u}_{\mathrm{pred}}^{n+1} - \frac{1}{2}\tau^2\big(\boldsymbol{F}^{1/2}\big(\boldsymbol{u}^n,\boldsymbol{u}^{n+1}\big) - \boldsymbol{F}_{\mathrm{con}}\big(\boldsymbol{u}^{n+1}\big) - \boldsymbol{F}_{\mathrm{fri}}\big(\boldsymbol{u}^{n+1}\big)\big) \tag{42}$$

$$\dot{\boldsymbol{u}}^{n+1} = \dot{\boldsymbol{u}}^n - \tau\big(\boldsymbol{F}^{1/2}\big(\boldsymbol{u}^n,\boldsymbol{u}^{n+1}\big) - \boldsymbol{F}_{\mathrm{con}}\big(\boldsymbol{u}^{n+1}\big)\big) \tag{43}$$

In a same manner as in (39) the dissipation of the algorithm in the frictional case can be proven, due to the implicit treatment of the contact and frictional stresses [21]. As the normal and tangential stresses influence each other, the stability of the normal stresses due to the predictor step is very important for the frictional effects. Numerical examples prove the stability of the frictional stresses. The arising discrete (quasi-)variational problems are solved with an efficient and robust non-smooth multiscale method for Coulomb friction [19,21]. Therein the non-linearities are resolved directly without any dependency on penalty parameters.

4. Comparison and interpretation of the basic ideas of the presented algorithms

The classical Newmark scheme with $2\beta = \gamma = 1/2$ leads to oscillations in the energy for contact problems. In [11] Kane et al. use the classical Newmark scheme with purely implicit treatment of the contact forces (see also [26]). It can be proven that this method is dissipative. But unfortunately there are still oscillations in the contact forces. Deuflhard et al. [4] improve this contact-implicit Newmark method in view of the oscillations in the contact forces. One explanation for these oscillations is the interplay of the discretization in space and time. In the continuous case the force $\boldsymbol{F}$ has to be equilibrated by means of the contact force $\boldsymbol{F}_{\mathrm{con}}$ such that penetration is avoided. After discretization in space and time we have an additional artificial force $\frac{2}{\tau^2}\boldsymbol{M}(\boldsymbol{u}_{\mathrm{rel}}^n + \tau\dot{\boldsymbol{u}}_{\mathrm{rel}}^n)$, see (23) which has to be equilibrated by $\boldsymbol{F}_{\mathrm{con}}$ if it provokes penetration but which has no direct physical meaning. In [4] an additional predictor step which avoids the appearance of these unphysical contact forces is introduced. Numerical examples show a stable behavior of the contact forces.

From the point of view of Khenous et al. [14] it is not simply the interaction of the time and space discretization which evokes the oscillations but the special energy conserving property of the time discretization in the unconstrained case together with the discretization in space. If for example a node is stopped at the contact boundary, its kinetic energy would be definitely lost. Thus, the energy conserving scheme makes the velocities oscillate (24) to keep the corresponding part of the kinetic energy. Consequently, not only the velocities oscillate but also the displacements, the energy and especially the contact forces. Khenous et al. remove the mass from the contact boundary. This method reduces the oscillations in the contact forces significantly. But setting up the discrete system requires additional numerical effort as the redistributed mass matrix is computed via a minimization problem under constraints. In contrast, the predictor step in [4] only requires a discrete $\boldsymbol{L}^2$-projection onto the discrete admissible set. Moreover the discrete $\boldsymbol{L}^2$-projection can easily be applied also in the case of changing spatial discretizations, which means that the discretization can take place first in time, second in space with adaptive refinement in each time step. This is not the case in [14]; they use the method of lines. In both methods numerical examples (in [14] and [21]) show that the energy tends to be conserved for smaller and smaller time steps. But in the algorithm of Deuflhard et al. the dissipativity can be proven.

Laursen and Chawla allow the penetration of the bodies in order to get energy conservation [23]. At points, where the two bodies penetrated each other in the foregoing time step further penetration is stopped by enforcing the discrete persistency condition. The discrete persistency condition implies that the difference quotient is zero at contacting points and therefore the energy is conserved. The simultaneous treatment of the non-penetration condition and the persistency condition seems to be a too great demand in the discrete setting. A discrete persistency condition can be fulfilled if the two bodies are allowed to penetrate each other, whereby smaller time-step sizes cause less penetration.

As this method conserves the energy exactly and the mass redistribution method of Khenous et al. reduces the oscillations in the contact forces, Hager et al. [9] combine both ideas and introduce a new less expensive method to compute a redistributed mass matrix. They also use the method of lines which does not allow for adaptive refinement in space.

A completely different idea was introduced by Laursen and Love. They add a discrete contact-related correction to the velocities at the contact boundary in such a way that the energy is conserved. In contrast to the algorithm of Laursen and Chawla the non-penetration condition is fulfilled. The motivation for the discrete contact-related correction of the velocities is the analysis of a waveform solution for a one-dimensional elastic impact where the contact effects are not only described in terms of the contact forces as usual for dynamic contact problems but also in terms of the velocities at the contact

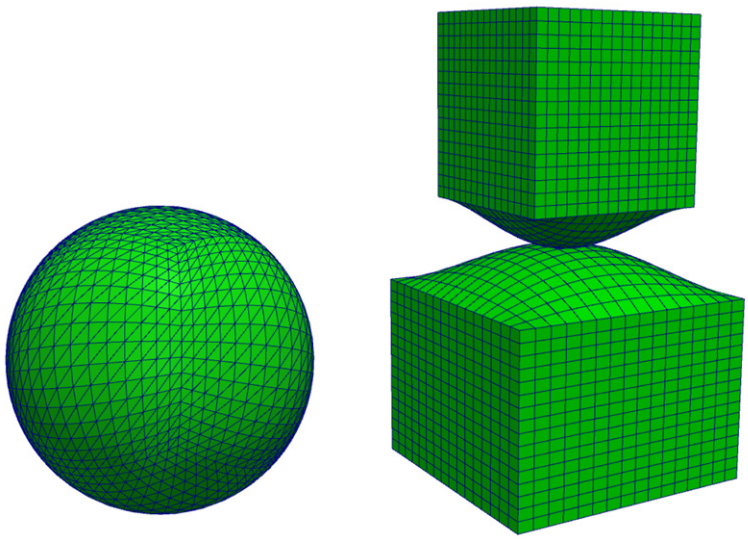

(a) Geometry **A** (b) Geometry **B**

Fig. 1. Meshes.

boundary. Further in dynamic contact problems there is a discrete change in the velocities at the contact boundary which of course cannot be reflected by a classical time discretization based on Taylor expansion.

The different authors use different solution methods for the solution of the inequalities. Hager et al. use a primal–dual active set strategy. Laursen et al. use penalty or augmented Lagrangian methods. These methods depend on the choice of algorithmic parameters. On the contrary the convergence of the monotone multigrid method used in [4] does not depend on any algorithmic parameter. In [18] it is shown that the monotone multigrid is a very efficient and robust solver.

All the algorithms are extended to frictional contact, except the one of Khenous et al. [14].

5. Numerical comparison

We consider numerical simulations to demonstrate the behavior of the different presented algorithms. Therefore, we implemented the algorithms for linear elastic one- and two-body contact problems in 3D, although mostly 2D examples are found in the original literature. First we show numerical examples for the classical Newmark scheme, the contact-implicit Newmark scheme (Algorithm 5), the contact-stabilized Newmark scheme (Algorithm 6), Algorithm 1 enforcing a discrete persistency condition and for different algorithms using a redistribution of the mass matrix (as Algorithm 3 and Algorithm 4). Then we comment on the similarities and differences, the advantages and disadvantages of the methods. The only algorithm which is left out in the numerical comparison is Algorithm 2, with the contact-related correction in the velocity, because there are several possible choices of the contact-related velocity, such that it makes no sense to take one and to compare it to the other algorithms.

The implementation has been carried out within the framework of the finite element toolbox `UG` [1] and the obstacle toolbox `OBSLIB++` [18]. Therein the discrete variational inequalities are solved with a monotone multigrid method which treats the non-linearities efficiently [16,18,17].

As there is no analytical solution for a three-dimensional dynamic contact problem in linear elasticity, we cannot compare the numerical and analytical solutions to validate the algorithm. Therefore, we are interested in the physical behavior of the system, which is reflected by displacements, velocities, energy and contact forces. In the foregoing sections we analyzed and compared the different algorithms and figured out that the temporal evolutions of energy, contact forces and contact stresses and closely connected to it the behavior of the velocity at the contact boundary are crucial points to examine.

For the numerical examples we use two different geometries, see Fig. 1.

The unit ball, Geometry **A**, consists of a four times uniformly refined mesh of pyramids and is used for one-body contact problems, meaning that the ball comes in contact with a rigid foundation. The initial distance to the foundation is zero at the south pole. Geometry **B** is used for two-body contact problems. The side lengths of the cubes are 1.4 and 1.0, respectively. The mesh of hexahedrons is also four times uniformly refined and the initial distance between the two bodies at their closest point is zero. All the materials are described by Hooke's law (1) for homogeneous isotropic material with the tensor

$$E_{ijkl} = \frac{E}{2(1+\nu)}(\delta_{ik}\delta_{jl} + \delta_{il}\delta_{jk}) + \frac{E\nu}{(1+\nu)(1-2\nu)}\delta_{ij}\delta_{kl} \tag{44}$$

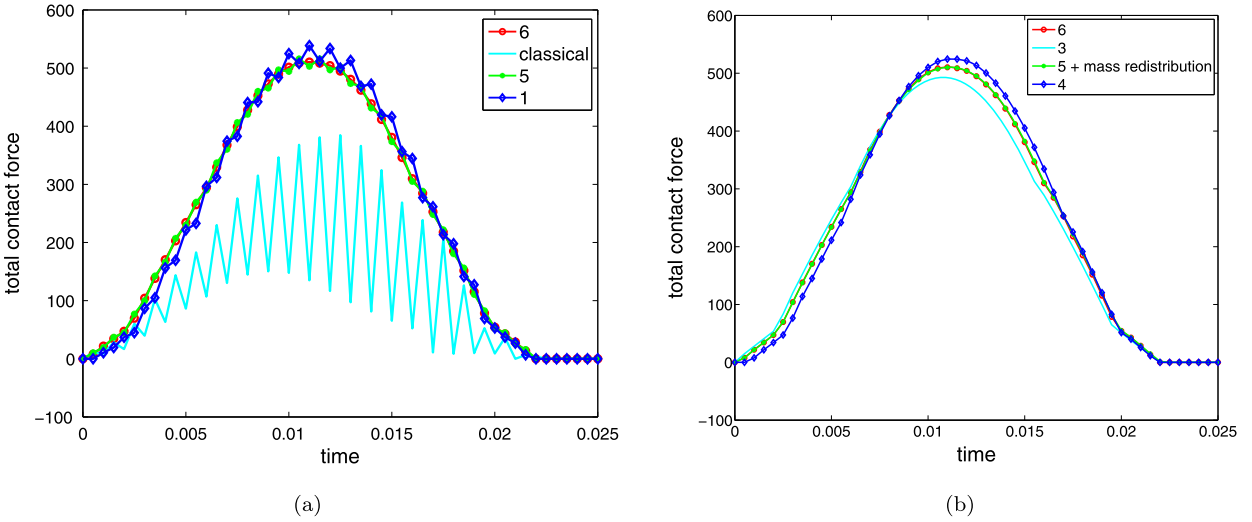

Fig. 2. Total contact force. (For interpretation of the references to color, the reader is referred to the web version of this article.)

where $\nu = 0.3$ and $E = 2 \cdot 10^5$ in Geometry **B** or $E = 5 \cdot 10^2$ in Geometry **A**. The initial velocity in vertical direction is -2 for the ball in the one-body contact problem and -2 for the upper body and 2 for the lower body in the two-body contact problem. We do not apply volume forces which means that $\boldsymbol{f} = \boldsymbol{0}$. The time step size is $\tau = 5 \cdot 10^{-3}$ for the one-body contact problem and $\tau = 5 \cdot 10^{-4}$ for the two-body contact problem.

5.1. Numerical results for the classical Newmark scheme

We start with the classical Newmark scheme for the two-body contact problem. In all the figures the corresponding line is denoted by "classical". In Fig. 3(a) the cyan colored line indicates the corresponding course of energy. The increase is up to 3.5% of the initial amount. The blue line with diamonds in Fig. 4(a) shows the trajectory of the relative displacement $\boldsymbol{u}_{\mathrm{rel}}^{n+1}$ and the blue line with diamonds in Fig. 5(a) shows the trajectory of the relative velocity $\dot{\boldsymbol{u}}_{\mathrm{rel}}^{n+1}$ of an arbitrarily chosen point which gets into contact. In the beginning the relative velocity shows the uniform zigzagging as expected from (24). In the end, when the points bounce and finally detach, the zigzagging is irregular. Here the increase of the energy may play a role. Even the displacements show some irregularities during and after the process of detaching. The development of the total contact force is shown in Fig. 2(a) indicated by the cyan colored line. To have a closer look at the behavior of the contact stresses, we show in Fig. 6(a) the contact stresses in an arbitrarily chosen time step. As we want to exclude undesirable effects stemming from the mortar method, the contact stresses are taken from the one-body contact problem with $E = 5 \cdot 10^2$.

5.2. Numerical results for the contact-implicit Newmark scheme (Algorithm 5)

The numerical results for the contact-implicit Newmark scheme are denoted by "5" corresponding to Algorithm 5. In Fig. 3(a) the green dotted line shows the course of energy for the two-body contact problem using the contact-implicit Newmark scheme of Kane et al. As stated in Section 3.5 this method is dissipative. The relative loss of energy is around 0.16%. Most of the loss of energy is due to the moment of impact. Similar as in the classical Newmark scheme we still have the oscillations in the relative velocities (see green line with dots in Fig. 5(a)). This can be calculated in the same way as in (24). But in contrast to the classical Newmark scheme during the process of detaching there is no bouncing in the relative displacements (see Fig. 4(a), green line with dots) and the amplitudes of the oscillations are more moderate. In the classical Newmark scheme the relative velocity oscillates between -12 and 12, whereas in the contact-implicit Newmark scheme the largest oscillation after the detaching is between 2 and 5. The development of the total contact force is shown in Fig. 2(a) indicated by the green line with dots. There are still oscillations but the amplitude is very small compared to the classical Newmark scheme. Fig. 6(b) shows the contact stresses at an arbitrarily chosen time step for the one-body contact problem with $E = 5 \cdot 10^2$. Oscillations can be observed, where the contact stresses are large.

5.3. Numerical results for the contact-stabilized Newmark scheme (Algorithm 6)

The lines illustrating the behavior of the contact-stabilized Newmark scheme in the different figures are denoted with "6" corresponding to Algorithm 6. In Fig. 3(a) (red line with circles) the dissipative behavior (39) of the contact-stabilized Newmark scheme of Deuflhard et al. can be seen. The system looses more energy during the process of detaching than during the impact. The loss of energy is around 0.4%. In Section 3.5, we explained that due to the predictor step the

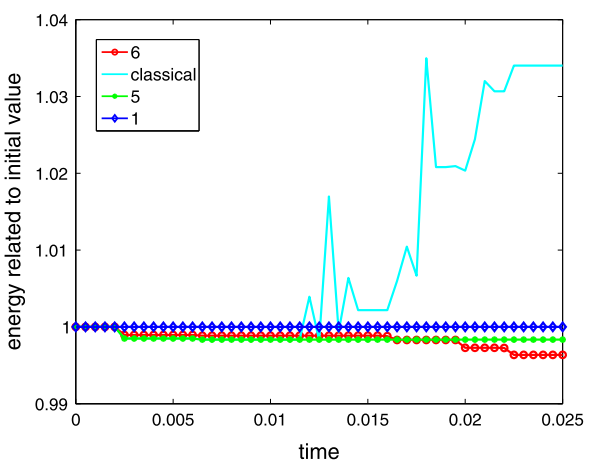

(a) $\mathcal{E} = \frac{1}{2}\dot{\boldsymbol{u}}\boldsymbol{M}\dot{\boldsymbol{u}} + \frac{1}{2}\boldsymbol{u}\boldsymbol{A}\boldsymbol{u}$

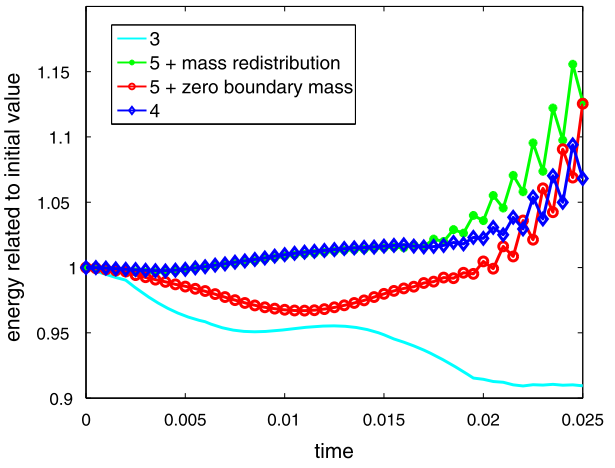

(b) $\mathcal{E} = \frac{1}{2}\dot{\boldsymbol{u}}\boldsymbol{M}\dot{\boldsymbol{u}} + \frac{1}{2}\boldsymbol{u}\boldsymbol{A}\boldsymbol{u}$

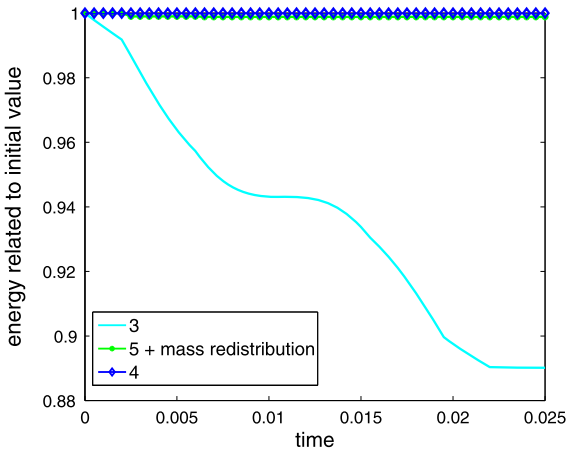

(c) $\tilde{\mathcal{E}} = \frac{1}{2}\dot{\boldsymbol{u}}\tilde{\boldsymbol{M}}\dot{\boldsymbol{u}} + \frac{1}{2}\boldsymbol{u}\boldsymbol{A}\boldsymbol{u}$

Fig. 3. Energy related to initial value. (For interpretation of the references to color, the reader is referred to the web version of this article.)

zigzagging of the relative velocities during contact is removed. The relative velocity remains the same during contact. But after detaching there are some oscillations. This can be seen in Fig. 5(a) (red line with circles). As expected from the name of the method the contact forces do not show any oscillations (Fig. 2(a), red line with circles).

The smooth behavior of the contact stresses is shown in Fig. 6(c) for the numerical example of the one-body contact problem with $E = 5 \cdot 10^2$.

5.4. Numerical results for Algorithm 1

The Algorithm 1 of Laursen and Chawla (denoted as "1" in all the figures) is the contact-implicit Newmark scheme with the discrete persistency condition as constraint instead of the non-penetration condition. Therefore, the energy is conserved (blue line with diamonds in Fig. 3(a)). The trajectory of the relative displacement Fig. 4(b) (cyan colored line with circles) reminds of the contact-implicit and contact-stabilized Newmark scheme, but the relative displacements evoke penetration of the two bodies as the non-penetration condition is not enforced. The straight red line indicates the initial gap at the chosen node. The behavior of the relative velocity, Fig. 5(b) (red line with circles) also reminds of the contact-implicit Newmark scheme but the amplitudes are larger. In Algorithm 1 the constraints $\boldsymbol{u}_{\mathrm{rel}}^{n+1} \cdot \boldsymbol{\nu} \leqslant \boldsymbol{u}_{\mathrm{rel}}^{n} \cdot \boldsymbol{\nu}$ have to be enforced when contact or penetration has occurred in the previous time step. Therefore, $\boldsymbol{u}_{\mathrm{rel}}^{n+1} \cdot \boldsymbol{\nu} = \boldsymbol{u}_{\mathrm{rel}}^{n} \cdot \boldsymbol{\nu}$ whenever the constraint in time step $n+1$ is active. Substituting this in (24) leads to $\dot{\boldsymbol{u}}_{\mathrm{rel}}^{n+1} \cdot \boldsymbol{\nu} = -\dot{\boldsymbol{u}}_{\mathrm{rel}}^{n} \cdot \boldsymbol{\nu}$ which means that the amplitude of the oscillation corresponds to the amount of the relative velocity before contact occurred. The temporal evolution of the contact forces (Fig. 2(a), blue line with diamonds) and contact stresses (Fig. 6(d)) are worse in the sense of more oscillations and larger amplitudes than for the contact-implicit Newmark scheme but still better than for the classical Newmark scheme.

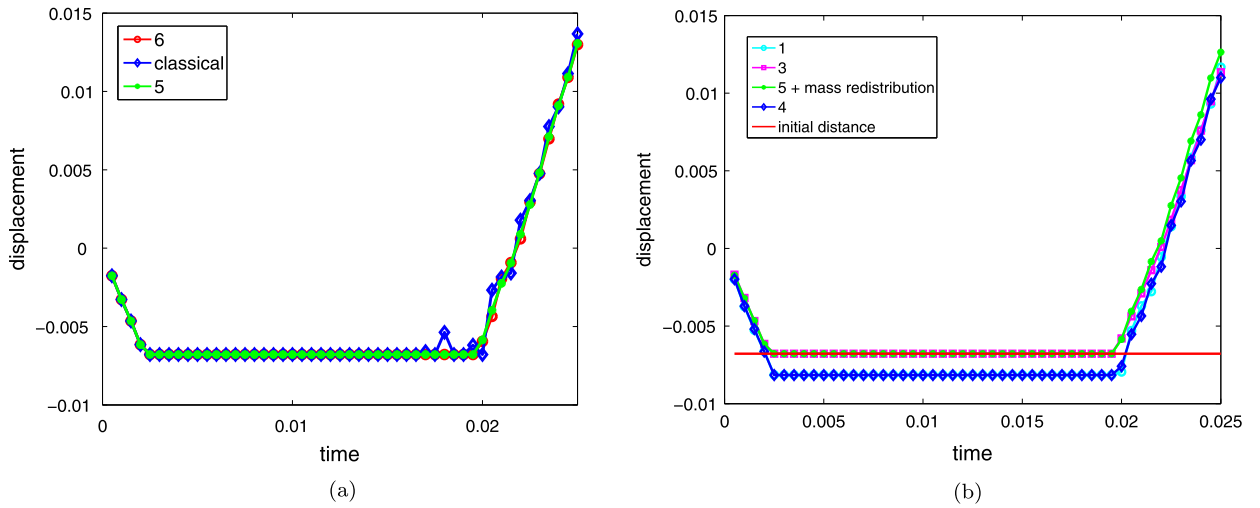

Fig. 4. Relative displacement. (For interpretation of the references to color, the reader is referred to the web version of this article.)

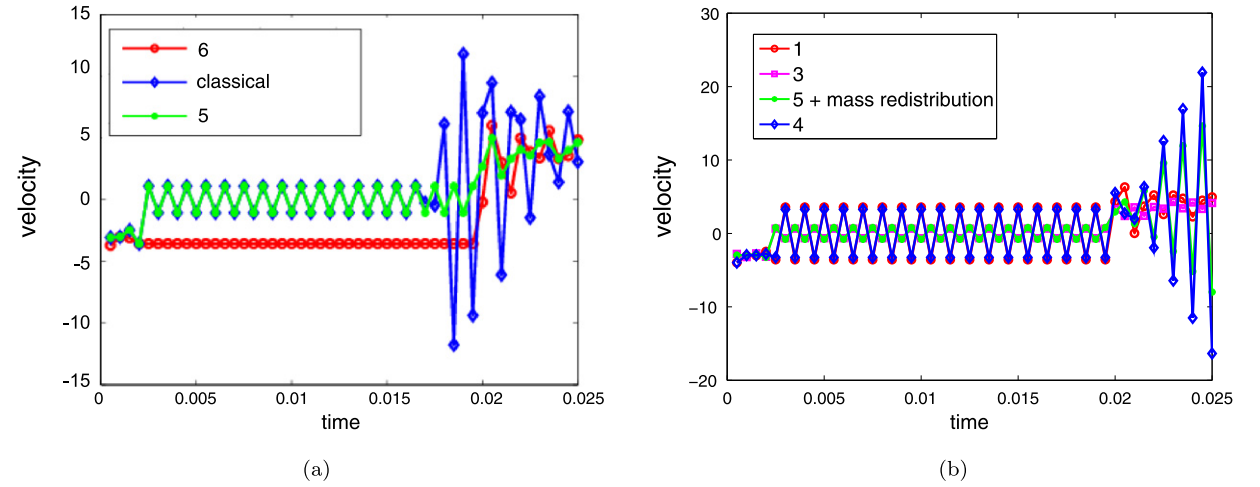

Fig. 5. Relative velocity. (For interpretation of the references to color, the reader is referred to the web version of this article.)

5.5. *Numerical results for the algorithms using a redistribution of the mass matrix*

In this subsection, we deal with three different algorithms using the idea of the redistributed mass, as firstly proposed in [13]. Therein Khenous et al. use a Newmark scheme with the parameters $\beta = \gamma = 1/2$, see Algorithm 3. However, Algorithm 4 of Hager et al. is the contact-implicit Newmark scheme with a redistributed mass and combined with Algorithm 1, which means that in the unconstrained case the algorithm corresponds to the classical Newmark scheme with the parameters $2\beta = \gamma = 1/2$ as in all the other presented methods. Therefore, we first investigate Algorithm 3, then the contact-implicit Newmark scheme with redistribution of the mass, which is Algorithm 4 with the non-penetration condition instead of the persistency condition and finally Algorithm 4 with the persistency condition.

For the computation of the redistribution of the mass matrix, such that the whole mass of the system and the center of gravity are conserved we use an Uzawa method.

In all the three subsequent algorithms we consider two different ways to compute the kinetic energy which is part of the whole energy. Usually the kinetic energy is computed as $\mathcal{E}_{\text{kin}} = \frac{1}{2}\dot{\boldsymbol{u}}\boldsymbol{M}\dot{\boldsymbol{u}}$, where $\boldsymbol{M}$ is the standard mass matrix. However, in [9] the kinetic energy was computed with the help of the redistributed mass matrix $\tilde{\boldsymbol{M}}$, $\tilde{\mathcal{E}}_{\text{kin}} := \frac{1}{2}\dot{\boldsymbol{u}}\tilde{\boldsymbol{M}}\dot{\boldsymbol{u}}$, which means that the velocities at the potential contact boundary are simply ignored, whereas the strains are taken into account for the elastic energy, because the stiffness matrix corresponds to the standard mass matrix $\boldsymbol{M}$. As long as a node remains in contact, the displacements do not change and therefore the difference quotient $\frac{1}{\tau}(\boldsymbol{u}_{\text{rel}}^{n+1} \cdot \boldsymbol{\nu} - \boldsymbol{u}_{\text{rel}}^{n} \cdot \boldsymbol{\nu})$ is zero, but the algorithms provide non-zero velocities, see Fig. 4(b). Even at nodes which are not actually in contact the velocities are ignored. We define $\tilde{\mathcal{E}} := \tilde{\mathcal{E}}_{\text{kin}} + \mathcal{E}_{\text{ela}}$.

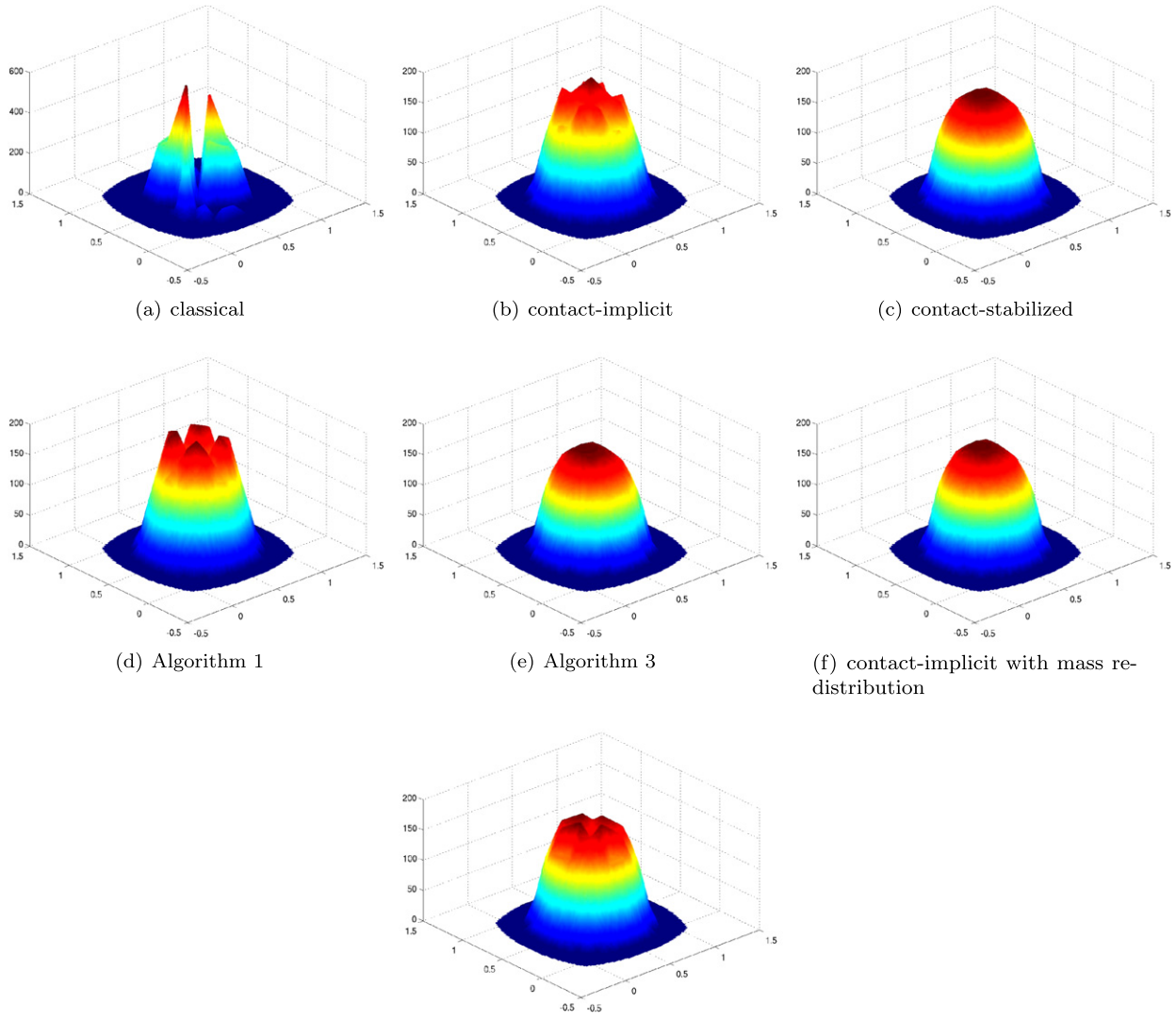

(a) classical (b) contact-implicit (c) contact-stabilized

(d) Algorithm 1 (e) Algorithm 3 (f) contact-implicit with mass redistribution

(g) Algorithm 4

Fig. 6. Contact stresses at time step 37.

5.5.1. Algorithm 3

The whole energy $\tilde{\mathcal{E}}$ relative to the initial amount is shown in Fig. 3(c) by the cyan colored line. Although there is no proof of dissipativity for this algorithm, the energy always decreases in this numerical example. The relative loss of energy amounts to 11.5%, which is a lot compared to the other presented algorithms. The course of the energy $\mathcal{E}$ relative to the initial amount can be seen in Fig. 3(b) by the cyan colored line. The loss of energy amounts to nearly 9% of the initial amount. It is not always dissipative. The behavior of the relative velocity (Fig. 5(b), magenta colored line with squares) is very similar to the contact-implicit Newmark scheme. The evolution of the contact forces and contact stresses, respectively, is smooth, which can be seen in Fig. 2(b) (cyan colored line) and Fig. 6(e).

5.5.2. Contact-implicit Newmark scheme with mass redistribution

Results concerning the contact-implicit Newmark scheme (Algorithm 5) with mass redistribution are indicated by "5 + mass redistribution". The energy $\tilde{\mathcal{E}}$ related to the initial value can be seen in Fig. 3(c) (green line with dots). The loss of energy is up to 0.12%. In contrast the energy $\mathcal{E}$ increases heavily up to 15%, see Fig. 3(b) (green line with dots). In order to check if the redistribution of the mass to the interior is responsible or not for this energy blow-up we make another experiment replacing $\tilde{\boldsymbol{M}}$ in the algorithm by the standard mass matrix with zero entries at the boundary but without redistribution of the mass. Therefore, we observe a similar behavior in the course of energy, see Fig. 3(b) (red line with circles indicated by "5 + zero boundary mass"). The green lines with dots in Figs. 4(b) and 5(b) shows the trajectories of the relative displacements and velocities at a fixed node. After detaching the amplitude of the oscillations in the relative

velocity at the contact boundary is very large. Similar to the foregoing algorithm the contact forces (green line with dots in Fig. 2b), and contact stresses, Fig. 6(f), are smooth.

5.5.3. Algorithm 4

Now we come to the algorithm of Hager et al. (Algorithm 4, referred to by "4" in the plots). As they enforce the persistency condition the energy is conserved at least as long as the kinetic energy is computed with the redistributed mass matrix, see blue line with diamonds in Fig. 3(c). Energy conservation does not hold if we use the standard mass matrix for the computation of the kinetic energy, see blue line with diamonds in Fig. 3(b). The energy blow-up amounts up to 10%. As in the algorithm of Laursen and Chawla the displacements evoke penetration (blue line with diamonds in Fig. 4(b)). The red straight line is the initial distance between the two bodies at the observed node. During contact the amplitude of the oscillations of the relative velocity (blue line with diamonds in Fig. 5(b)) at the contact boundary is the same as in Algorithm 1 but after detaching the amplitude tops any of the other algorithm as the value of the relative velocity in normal direction changes between -18 and 22. The total contact forces, blue line with diamonds in Fig. 2(b), are smooth, but if we have a closer look at the contact stresses for the one-body contact problem the stresses show slight oscillations, Fig. 6(g).

5.6. Conclusion

In this subsection we give some more detailed comments on the numerical results obtained above.

Apart from the classical Newmark scheme all the algorithms show a similar behavior of the relative displacements at contact nodes. But in Algorithms 1 and 4 the non-penetration condition is violated. Using the classical Newmark scheme we observe some kinks in the process of detaching.

In all the algorithms the relative velocities at the contact boundary show oscillations at some time. The contact-stabilized Newmark scheme is the only one which does not evoke oscillations in the relative velocities during contact. Once a node is in contact the relative velocity remains the same. After detaching there are a few oscillations as in the contact-implicit Newmark scheme, Algorithm 1 and Algorithm 3. The other algorithms show more oscillations with larger amplitudes after detaching, especially Algorithm 4. During contact the two algorithms enforcing the discrete persistency condition instead of the non-penetration condition evoke oscillations in the relative velocities, which have an amplitude of the amount of the relative velocities before contact occurred. This numerical observation can be easily verified by reformulating the velocity update $\dot{\boldsymbol{u}}^{n+1} = -\dot{\boldsymbol{u}}^n + \frac{2}{\tau}(\boldsymbol{u}^{n+1} - \boldsymbol{u}^n)$ and exploiting $\boldsymbol{u}_{\mathrm{rel}}^{n+1} \cdot \boldsymbol{\nu} = \boldsymbol{u}_{\mathrm{rel}}^{n} \cdot \boldsymbol{\nu}$, whenever constraints are active. For all other algorithms the amplitude of the relative velocity is less or equal to the amount of the relative velocity before contact occurred. Unfortunately none of the investigated algorithms shows the desirable behavior of the relative velocities, which should be zero in the case of contact to fulfill the persistency condition.

The behavior of the velocities influences the energy. The energy of the classical Newmark scheme oscillates and increases up to 3.5% in our example, whereas the contact-implicit and contact-stabilized Newmark schemes are provably dissipative. The relative loss of energy amounts to 0.16% and 0.4%. In Algorithm 1 the energy is conserved because the discrete persistency condition is enforced. The same holds for Algorithm 4 as long as the kinetic energy is computed with the redistributed mass matrix. Depending on whether the kinetic energy is computed with the standard or the redistributed mass matrix the energy may increase or decrease in the different algorithms employing a redistribution of the mass matrix.

The total contact forces show a smooth behavior for the contact-stabilized Newmark scheme and all variants of algorithms using a redistribution of the mass matrix (see Fig. 2(b)). The contact stresses reflect this stable behavior, except for Algorithm 4, where the persistency condition is enforced. There are slight oscillations in the contact stresses. Using the contact-implicit Newmark scheme we observe some oscillations in the contact stresses and forces. In Algorithm 1 there are even more oscillations and of course the classical Newmark scheme shows so much oscillations with such large amplitudes that one can hardly recognize the real behavior.

Acknowledgements

The authors would like to thank Thomas Dickopf for carefully reading and the Deutsche Forschungsgemeinschaft (SFB 611, Hausdorff Center for Mathematics and Bonn International Graduate School) for various financial support.

References

[1] P. Bastian, K. Birken, S. Lang, N. Neuss, H. Rentz-Reichert, C. Wieners, UG – A flexible software toolbox for solving partial differential equations, Computing and Visualization in Science 1 (1997) 27–40.
[2] V. Chawla, T. Laursen, Energy consistent algorithms for frictional contact problems, International Journal for Numerical Methods in Engineering 42 (1998) 799–827.
[3] P. Ciarlet, Mathematical Elasticity, vol. 1: Three Dimensional Elasticity, North-Holland, Amsterdam, 1988.
[4] P. Deuflhard, R. Krause, S. Ertel, A contact-stabilized Newmark method for dynamical contact problems, International Journal for Numerical Methods in Engineering 73 (9) (2008) 1274–1290.
[5] T. Dickopf, R. Krause, Efficient simulation of multi-body contact problems on complex geometries: a flexible decomposition approach using constrained minimization, International Journal for Numerical Methods in Engineering 77 (13) (2009) 1834–1862.
[6] C. Eck, Existenz und Regularität der Lösungen für Kontaktprobleme mit Reibung, Ph.D. thesis, Mathematisches Institut der Universität, Stuttgart, 1996.
[7] C. Eck, J. Jarusek, M. Krbec, Unilateral Contact Problems. Variational Methods and Existence Theorems, Chapman and Hall/CRC, 2005.

[8] I. Ekeland, R. Temam, Convex Analysis and Variational Problems, North-Holland Publishing Company, 1976.
[9] C. Hager, S. Hüeber, B. Wohlmuth, A stable energy conserving approach for frictional contact problems based on quadrature formulas, International Journal for Numerical Methods in Engineering 73 (2008) 205–225.
[10] E. Hairer, C. Lubich, G. Wanner, Geometric numerical integration. Structure-preserving algorithms for ordinary differential equations, in: Computational Mechanics, Springer, Berlin, Heidelberg, 2006.
[11] C. Kane, E. Repetto, M. Ortiz, J. Marsden, Finite element analysis of nonsmooth contact, Computer Methods in Applied Mechanics and Engineering 180 (1999) 1–26.
[12] H. Khenous, P. Laborde, Y. Renard, On the discretization of contact problems in elastodynamic, Lecture Notes in Applied and Computational Mechanics 27 (2006) 31–38.
[13] H. Khenous, P. Laborde, Y. Renard, A energy conserving approximation for elastodynamic contact problems, 3rd., in: C.A. Mota Soares et al. (Eds.), European Conference on Computational Mechanics, Solids Structures and Coupled Problems in Engineering, 2006.
[14] H. Khenous, P. Laborde, Y. Renard, Mass redistribution method for finite element contact problems in elastodynamics, European Journal of Mechanics A – Solids 27 (5) (2008) 918–932.
[15] N. Kikuchi, J. Oden, Contact Problems in Elasticity: A Study of Variational Inequalities and Finite Element Methods, SIAM, Philadelphia, 1988.
[16] R. Kornhuber, Adaptive Multigrid Methods for Nonlinear Variational Problems, Teubner-Verlag, 1997.
[17] R. Kornhuber, R. Krause, Adaptive multigrid methods for Signorini's problem in linear elasticity, Computing and Visualization in Science 4 (2001) 9–20.
[18] R. Krause, Monotone multigrid methods for Signorini's problem with friction, Ph.D. thesis, Freie Universität, Berlin, 2000.
[19] R. Krause, A non-smooth multiscale method for solving frictional two body contact problems in 2D and 3D with multigrid efficiency, SIAM Journal on Scientific Computing 31 (2) (2009) 1399–1423.
[20] R. Krause, C. Mohr, Level set based multi-scale methods for large deformation contact problems, Applied Numerical Mathematics 61 (4) (2011) 428–442.
[21] R. Krause, M. Walloth, A time discretization scheme based on Rothe's method for dynamical contact problems with friction, Computer Methods in Applied Mechanics and Engineering 199 (2009) 1–19.
[22] T. Laursen, Computational Contact and Impact Mechanics, Springer, Berlin, Heidelberg, New York, 2002.
[23] T. Laursen, V. Chawla, Design of energy conserving algorithms for frictionless dynamic contact problems, International Journal for Numerical Methods in Engineering 40 (1997) 863–886.
[24] T. Laursen, G. Love, Improved implicit integrators for transient impact problems – geometric admissibility within the conserving framework, International Journal for Numerical Methods in Engineering 53 (2) (2002) 245–274.
[25] G. Love, T. Laursen, Improved implicit integrators for transient impact problems – Dynamic frictional dissipation within an admissible conserving framework, Computer Methods in Applied Mechanics and Engineering 192 (2003) 2223–2248.
[26] A. Pandolfi, C. Kane, J.E. Marsden, M. Ortiz, Time-discretized variational formulation of non-smooth frictional contact, International Journal for Numerical Methods in Engineering 53 (2002) 1801–1829.
[27] J. Simo, N. Tarnow, The discrete energy–momentum method. Conserving algorithms for nonlinear elastodynamics, Zeitschrift für angewandte Mathematik und Physik 43 (5) (1992) 757–792.
[28] B. Wohlmuth, A mortar finite element method using dual spaces for the Lagrange multiplier, SIAM Journal of Numerical Analysis 38 (3) (2000) 989–1012.
[29] B. Wohlmuth, R. Krause, Monotone methods on nonmatching grids for non linear contact problems, SIAM Journal on Scientific Computing 25 (1) (2003) 324–347.
[30] P. Wriggers, Computational Contact Mechanics, J. Wiley & Sons, 2002.